

## Article

# Spatiotemporal Variability of Groundwater Quality for Irrigation: A Case Study in Mimoso Alluvial Valley, Semiarid Region of Brazil

Thayná A. B. Almeida <sup>1</sup>, Abelardo A. A. Montenegro <sup>1</sup>, João L. M. P. de Lima <sup>2,\*</sup>, Carolyne W. L. A. Farias <sup>3</sup>, Ailton A. Carvalho <sup>4</sup> and Anderson L. R. de Paiva <sup>5</sup>

<sup>1</sup> Department of Agricultural Engineering, Federal Rural University of Pernambuco State, Recife 52171-900, PE, Brazil; thayna.britoalmeida@ufrpe.br (T.A.B.A.); abelardo.montenegro@ufrpe.br (A.A.A.M.)

<sup>2</sup> MARE–Marine and Environmental Sciences Centre / ARNET–Aquatic Research Network, Department of Civil Engineering, Faculty of Sciences and Technology, University of Coimbra, Rua Luís Reis Santos, Pólo II–University of Coimbra, 3030-788 Coimbra, Portugal

<sup>3</sup> Department of Geosciences, Federal University of Paraíba, João Pessoa 58051-900, PB, Brazil; carolyne.andrade@academico.ufpb.br

<sup>4</sup> Academic Unit of Serra Talhada, Federal Rural University of Pernambuco, Serra Talhada 56909-535, PE, Brazil; ailtonalvess@hotmail.com

<sup>5</sup> Environmental and Civil Engineering Department, Federal University of Pernambuco State, UFPE, Recife 50740-467, PE, Brazil; anderson.paiva@ufpe.br

\* Correspondence: plima@dec.uc.pt

**Abstract:** Alluvial aquifers are vital for agricultural communities in semiarid regions, where groundwater quality is often constrained by seasonal and spatial salinity variations. This study employed geostatistical methods to analyze the spatial and temporal variability of electrical conductivity (EC) and the sodium adsorption ratio (SAR) and elaborate an indicative quality map in the Mimoso Alluvial Aquifer, Pernambuco, Brazil. Groundwater samples were collected and analyzed for cations, total hardness (TH), and the percentage of sodium (PS). Moreover, the relation between EC and the SAR was used to determine the groundwater quality for irrigation. Cation concentrations followed the order  $\text{Ca}^{2+} > \text{Mg}^{2+} > \text{Na}^+ > \text{K}^+$ . EC and the SAR exhibited medium to high variability, with spatial dependence ranging from moderate to strong, and presented a strong cross-spatial dependence. Results showed that sequential Gaussian simulation (SGS) provided a more reliable groundwater classification for agricultural purposes compared to kriging methods, enabling a more rigorous evaluation. Based on the strong geostatistical cross correlation between EC and RAS, a novel water quality index was proposed, properly identifying regions with lower groundwater quality. The resulting spatial indicator maps classified groundwater as suitable (64.7%), restricted use (2.08%) and unsuitable (2.38%) for irrigation. The groundwater quality maps indicated that groundwater was mostly suitable for agriculture, except in silty areas, also corresponding to regions with low hydraulic conductivity at the saturated zone. Soil texture, rainfall, and water extraction significantly influenced spatial and temporal patterns of groundwater quality. Such correlations allow a better understanding of the groundwater quality in alluvial valleys, being highly relevant for water resources management in semiarid areas.

**Keywords:** groundwater quality; electrical conductivity; SAR; geostatistical analysis; semiarid areas



Academic Editor: Christos S. Akrotos

Received: 3 December 2024

Revised: 11 January 2025

Accepted: 27 January 2025

Published: 1 February 2025

**Citation:** Almeida, T.A.B.; Montenegro, A.A.A.; de Lima, J.L.M.P.; Farias, C.W.L.A.; Carvalho, A.A.; de Paiva, A.L.R. Spatiotemporal Variability of Groundwater Quality for Irrigation: A Case Study in Mimoso Alluvial Valley, Semiarid Region of Brazil. *Water* **2025**, *17*, 410. <https://doi.org/10.3390/w17030410>

**Copyright:** © 2025 by the authors.

Licensee MDPI, Basel, Switzerland.

This article is an open access article distributed under the terms and conditions of the Creative Commons Attribution (CC BY) license

(<https://creativecommons.org/licenses/by/4.0/>).

## 1. Introduction

In semiarid regions, groundwater is an essential source of water, being crucial for the development of the region [1]. The reliance of irrigated agriculture in these regions on groundwater and its unrestricted use can lead to aquifer depletion and a deterioration in water quality [2]. The qualitative and quantitative availability of this resource is impacted by climatic variations, farming activities, and pumping [3,4]. The alluvial valleys of semiarid regions have a high potential for small-scale irrigation; however, they are prone to the build-up of salts in both the unsaturated and saturated zones, depending, among other factors, on the spatial distribution of their hydraulic characteristics [5].

Groundwater salinization is a recurrent and critical environmental and socioeconomic problem in semiarid regions. It is mainly caused by the interaction of water with rocks, hydrodynamic conditions, climatic events of precipitation and evapotranspiration, as well as human activities such as over-exploitation of underground resources and incorrect irrigation management [6–8]. Excessive abstraction of groundwater in recent decades has led to a decrease in water quality, and they also warn of the scarcity of studies on the availability of adequate water for irrigation [9]. Groundwater quality in semiarid alluvial valleys is highly variable seasonally due to the influences of hydrological and climatic conditions, such as the dilution of salts by rainfall recharge and the concentration of salts by greater evaporation of water in the dry season [10].

The salinization of groundwater presents a significant risk to human health and has a considerable impact on the environment [11,12]. This process can have detrimental consequences on various productive areas, leading to the infertility of agricultural soils [13]. Additionally, irrigating soils with low permeability using saline water can cause a gradual yet excessive build-up of salts in soils [6]. The quality of irrigation water is determined by several types of salts that contribute to its salinity and sodicity [2]. Electrical conductivity (EC) is an effective indicator of salinity, while the sodium adsorption ratio (SAR) is commonly used to assess the suitability of water for irrigation [14]. EC reflects the total amount of dissolved ions in the water, while the SAR indicates the proportion of dissolved sodium in relation to calcium and magnesium [15]. Examining various water quality parameters, such as EC and the SAR, can give a comprehensive understanding of groundwater quality and its suitability for irrigation [16].

To effectively manage and sustain agriculture, it is essential to be aware of the spatial variations in groundwater quality and its influencing factors [6]. The significance of assessing groundwater quality for proper water resource planning and management, which requires an accurate and reliable analysis and prediction model, has been underlined by several studies [17,18]. Geostatistics is a method largely used by researchers to spatially estimate groundwater parameters [19]. For example, the indicator kriging method was used to pinpoint suitable areas for irrigation systems in southern Iran, demonstrating the usefulness of geostatistical techniques for the spatial assessment of groundwater quality by mapping EC and the SAR [20]. Similarly employed geostatistical methods to ascertain the spatial distribution of groundwater quality parameters in Northeast Algeria, thus allowing the identification of groundwater suitability through the intersections between EC and the SAR kriging [14].

Although kriging provides good local accuracy, it is subject to uncertainties and tends to smooth variability, which can lead to underestimations of spatial variations in the estimated values compared to observed values. Additionally, it may not fully capture the spatial uncertainty inherent in the estimates [21,22]. On another hand, stochastic simulation techniques such as sequential Gaussian simulation (SGS) can generate alternative and equally probable realizations for spatial variables, considering the spatial variability of data at sampled locations and the variability of estimates at unsampled locations [23–25].

Stochastic realizations reduce the smoothing effect and can more accurately represent spatial heterogeneity. Recent studies have provided predictions of spatial heterogeneity through kriging, robust quantification of resulting uncertainty, and the probability of exceeding certain threshold concentration values through stochastic simulation in groundwater. SGS has also been used to evaluate the reliability of groundwater flow simulations to assess the heterogeneity of hydrogeological parameters [26–28].

Mimoso Alluvial Valley, located in the semiarid region of northeastern Brazil, is part of the Nossa Senhora do Rosário rural settlement, where small-scale agriculture is practiced using groundwater irrigation [4]. The region faces significant challenges related to groundwater salinity and sodicity, which directly threaten crop yields and soil health, exacerbating the already precarious conditions of agricultural sustainability. Previous studies have evaluated the saline dynamics of the aquifer, identifying spatiotemporal patterns of variability and spatial dependence in electrical conductivity (EC) through geostatistical techniques [4,10]. Despite these efforts, there remains a high level of uncertainty regarding the temporal dynamics of salinity, particularly its relationship with episodic recharge events and periods of intense evapotranspiration [29]. Additionally, the interplay between irrigation water quality and its spatiotemporal variability is poorly understood, leaving farmers with limited management alternatives to mitigate salinity risks effectively.

To address these gaps, this study aims to: (i) assess the groundwater quality in Mimoso Alluvial Valley by measuring soluble salts; (ii) map EC and the SAR using geostatistical methods, including kriging and sequential Gaussian simulation; (iii) propose a groundwater quality index for irrigation purposes; and (iv) identify areas with suitable groundwater quality for agriculture through the integration of these indicators. By providing a comprehensive analysis of the spatial and temporal dynamics of irrigation water quality, this research seeks to offer critical insights to improve water sustainability and support irrigated agriculture in the region.

## 2. Material and Methods

### 2.1. Study Area

This study was conducted in Mimoso Alluvial Valley (MAV), located in Alto Ipanema Basin, a smaller sub-basin of Ipanema River Basin in Pernambuco, northeastern Brazil (Figure 1). Covering an area of 100–136 hectares, the valley is bordered by the slopes of the crystalline basement and runs along the alluvial terrace of the Ipanema River. The main watercourse in the basin is the Mimoso River, an intermittent stream characteristic of semiarid regions, which is hydraulically connected to the aquifer along its entire length [5]. According to the Köppen classification, the climate in the region is BSsh (extremely hot and semiarid), with an average annual rainfall of 630 mm [4].

MAV has a shallow unconfined aquifer with an average thickness of approximately 10 m, approximately 3 km in length and 300 m in width, with a natural topographic slope of approximately 0.3% (West–East) [30]. The soil in the area is predominantly Fluvic Neosol, which is a heterogeneous deposit containing medium to high silt content [30].

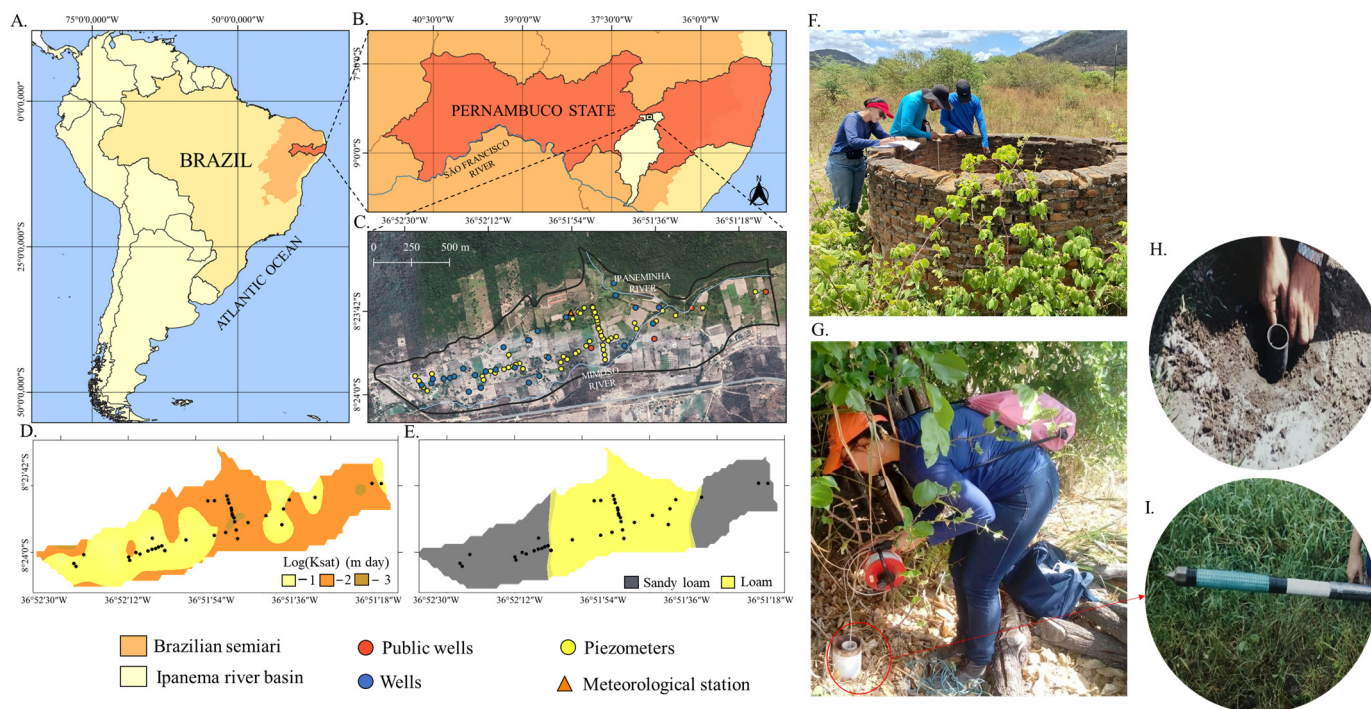


**Figure 1.** South America map, with location of the semiarid region in Brazil (A); Pernambuco State, and location of Ipanema River Basin (B); Mimoso Alluvial Valley, Alto Ipanema Basin, Pesqueira municipality of Pernambuco State, Brazil (C); saturated hydraulic conductivity map of Mimoso Alluvial Aquifer (D); soil surface texture map of Mimoso Alluvial Aquifer (E); well (F) and piezometers (G) monitoring; and piezometers installation (H,I).

Mimoso Alluvial Valley (MAV) consists of a narrow alluvial formation primarily composed of fine to medium sands with heterogeneous characteristics, mixed with varying amounts of silt and clay [30]. The sandy sediments are rich in coarse quartz particles and fragments of pink feldspar, along with the presence of biotite, muscovite, and gneiss minerals [4]. To the north, a granite complex, including granite, syenite, and gabbro, is found, which likely contributes quartz particles to the alluvial fans in the region. While soils in the crystalline terrains are generally shallow, with limited infiltration capacity and low water retention, the alluvial deposits differ significantly, offering higher porosity and greater hydraulic conductivity.

The hydraulic conductivity of the aquifer ranges from 0.1 to 125.0 m day<sup>-1</sup>, while the saturated hydraulic conductivity of the subsoil varies between 0.07 and 93.0 m day<sup>-1</sup>, with an average of 7.13 m day<sup>-1</sup> [4]. Loam and sandy-loam soils dominate the area, with loamy soils favoring capillary rise and surface accumulation of excess rainfall and irrigation water due to their low infiltration rates. Regional stratigraphy and hydrology significantly influence salinity and sodicity dynamics. In finer-textured soils, water tends to accumulate at or near the surface, leading to higher evaporation rates and potential salt accumulation.

Groundwater flow and salt transport pathways are monitored using wells and piezometers, classified based on hydraulic conductivity: low hydraulic conductivity (Log(K) ≤ 0.8 m day<sup>-1</sup>) and high hydraulic conductivity (Log(K) > 0.8 m day<sup>-1</sup>) [4].

On the surrounding slopes, soils of the Fluvisols, Regosols, Lithosols, Litholic, Regolitic Neosols, and Argisols types are present, with clayed lens as impediment layers. Saturated zone monitoring through piezometers [4] reveals that the average water table depth fluctuates between 2 and 4 m during the rainy and dry periods, respectively. The pedological classification [31] of the valley is as follows (Figure 2): RR1: Regolith Neosol + Litholic Neosol (both with a gently undulating phase); RR2: Regolith

Neosol (Eutrophic Solodic, medium (light) texture, with flat and gently undulating relief phases); RU1: Fluvic Neosol Eutric Medium Sand (Eutrophic Typical, sandy or medium (light) texture, moderately drained); RU2: Fluvic Neosol Eutric Medium (Eutrophic Typical, medium (light) texture, moderately drained); RU3: Fluvic Neosol Sodium Medium (Sodic Typical, medium (light) or sandy texture, moderately drained); RU4: Fluvic Neosol Sodic Medium Sand (Sodic Typical, medium or sandy texture, moderately drained); RU5: Fluvic Neosol Sodium Saline (Sodic Saline, medium or medium (light) texture, imperfectly drained); RU6: Fluvic Neosol Saline Sodium (Sodic Saline, medium texture, imperfectly drained).

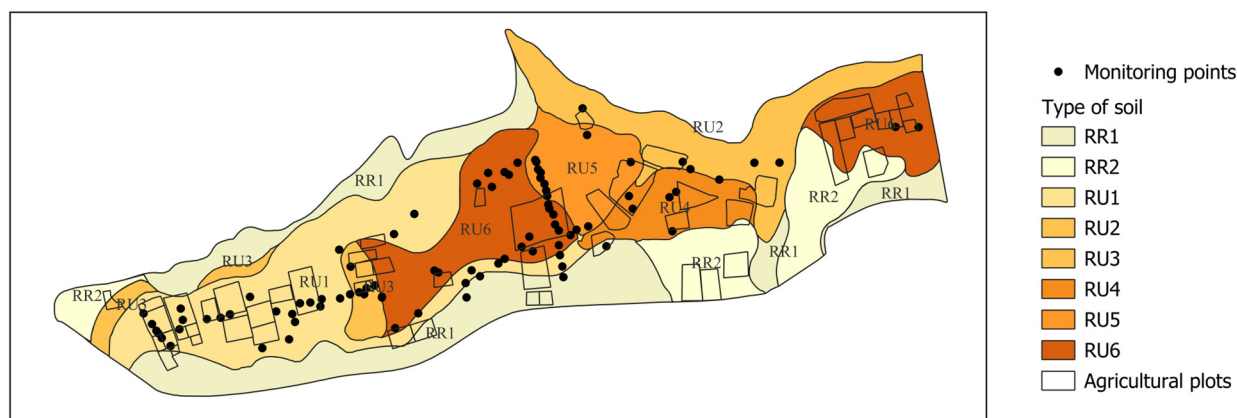


**Figure 2.** Soil map Location of Mimoso Alluvial Valley and locations of irrigated plots (adapted from [31]).

The most important economic activity in MAV is agriculture, with approximately 51 plots designated for family farming. Each irrigated plot is equipped with an irrigation system supplied by one of the monitoring wells used for analysis. The primary crops cultivated in the plots were: carrot (*Daucus carota* L.), cabbage (*Brassica oleracea* L. var. capitata L.), bell pepper (*Capsicum annum*), tomato (*Lycopersicon esculentum*), watermelon (*Citrullus lanatus*), coriander (*Coriandrum sativum*), gherkin (*Cucumis anguria*), and maize (*Zea mays*). To estimate water exploitation for irrigation in MAV, the actual consumption was considered for each farm and its respective farmers based on the water requirements of the irrigated crops [4].

## 2.2. Meteorological Data

The meteorological data were collected using a Campbell Scientific automatic weather station installed in MAV from 2000 to 2019. This station provided daily records of air temperature, relative humidity, global solar radiation, atmospheric pressure, wind speed and direction, and rainfall. Reference evapotranspiration was obtained from the climatological data recorded in the automatic station and calculated using the FAO Penman–Monteith method [32].

## 2.3. Groundwater Quality Data

For this study, 12 months of electrical conductivity data were collected from January 2000 to December 2019 from a network of 54 piezometers and 33 wells [4]. Due to decommissioning or disrepair of wells and piezometers, only 36 piezometers and 15 wells were considered. The piezometers had a mean depth of six meters and a 75 mm diameter, present screens and gravel filters. The wells, on the other hand, varied in size, comprising community wells with larger diameters and equipped with multilevel radial collectors aimed

at increasing groundwater exploitation, and individual wells for supplying individual irrigation plots.

The water samples were collected, transferred to a sealed container and packed in a thermal box. The sampling was conducted within the first 15 days of each month, with slight variations of 2 to 5 days between months, from 8 am to 2 pm. The conditions of sample collection varied according to the climatic conditions of each day. However, all procedures were standardized to ensure consistency: the equipment and instruments used during sampling, the storage temperature, and the time elapsed between sample collection and salt determination were maintained constant throughout this study. The electrical conductivity (EC) was read using a conductivity meter (HANNA-HI 9835, EMIN, Ha Noi City, Vietnam) adjusted to the sample temperature. The  $\text{Na}^+$  and  $\text{K}^+$  contents were determined by flame emission photometry and the  $\text{Ca}^{2+}$  and  $\text{Mg}^{2+}$  contents by titration in EDTA after the sample had been buffered, for the months of May to November. The total water hardness (TH) was calculated using Equation (1) [33].

$$\text{TH} = (\text{Ca}^{2+} + \text{Mg}^{2+}) + 50 \quad (1)$$

where  $\text{Ca}^{2+}$  = calcium concentration in  $\text{mmolc L}^{-1}$ ;  $\text{Mg}^{2+}$  = concentration of magnesium in  $\text{mmolc L}^{-1}$ .

The total water hardness results were categorized into four restriction levels [34]: mild ( $\text{TH} < 75$ ); moderate ( $75 < \text{TH} < 150$ ); high ( $150 < \text{TH} < 300$ ); and very high ( $\text{TH} > 300$ ). The percentage of sodium (SP) was used to assess the suitability of water for agricultural uses, being determined by Equation (2) [34], in which all variables are expressed in  $\text{mmolc L}^{-1}$ .

$$\text{SP} = \frac{\text{Na}^+}{\text{Ca}^{2+} + \text{Mg}^{2+} + \text{Na}^+ + \text{K}^+} \times 100 \quad (2)$$

where  $\text{Na}^+$ ,  $\text{K}^+$ ,  $\text{Ca}^{2+}$ ,  $\text{Mg}^{2+}$  correspond to the concentrations of sodium, potassium, calcium and magnesium in water, respectively, in  $\text{mmolc L}^{-1}$ .

The percentage of sodium was classified into five groups: very low ( $\text{SP} \leq 20$ ); low ( $20 < \text{SP} \leq 40$ ); moderate ( $40 < \text{SP} \leq 60$ ); high ( $60 < \text{SP} \leq 80$ ); and very high ( $\text{SP} > 80$ ). In the context of groundwater quality classification, the classification framework [35] served as the primary reference. The irrigation water classification was carried out in accordance with the SAR ( $\text{mmolc L}^{-1}$ )<sup>0.5</sup> [36], as shown in Equation (3).

$$\text{SAR} = \frac{\text{Na}^+}{\sqrt{\frac{\text{Ca}^{2+} + \text{Mg}^{2+}}{2}}} \quad (3)$$

where ion concentrations of  $\text{Na}^+$ ,  $\text{Ca}^{2+}$ , and  $\text{Mg}^{2+}$  are expressed in  $\text{mmolc L}^{-1}$ .

The categorization of irrigation water quality adhered to the framework introduced by the United States Salinity Laboratory, known as the Richards diagram [37]. In this classification, the parameters of electrical conductivity (indicative of salinity risk) and the sodium absorption ratio (SAR, indicative of sodium adsorption risk) are utilized. These parameter values are graphically represented on the diagram, which is partitioned into four discernible tiers, facilitating the systematic classification of water samples. Table 1 furnishes the elucidation of diagram classes, predicated upon the seminal work of Richards [36].

**Table 1.** Groundwater classification for irrigation purpose [36].

		Salinity			Sodicity
C1	Low	Can be used for most crops and on many soil types.	S1	Low	Suitable for use on almost all soil types.
C2	Medium	Can be used, provided that moderate leaching of salts occurs in the soil.	S2	Medium	May pose a risk of sodicity in fine-textured soils with low leaching rates.
C3	High	Should not be used on soils with drainage restrictions.	S3	High	May result in dangerous levels of exchangeable sodium in most soils.
C4	Very High	Not suitable for irrigation.	S4	Very High	Unsuitable for irrigation, except when salinity is low or medium.

The groundwater quality for the irrigation indicator (GWQ) categorizes water suitability for irrigation into four classes [36,37]. To develop this indicator for agricultural suitability, soil characteristics from the alluvial valley were considered, including soil type, hydraulic properties, salinization susceptibility, and texture.

#### 2.4. Geostatistical Methods

The statistical distribution of data was evaluated according to the normal distribution, using the Kolmogorov–Smirnov (KS) test, at a probability level of 0.05. The KS test is largely applied and appropriate for hydrogeological applications and environmental research, for sample sizes of at least 50 points. According to the coefficient of variation (CV) values, variability was classified as low ( $CV \leq 12\%$ ); medium ( $12 < CV \leq 60\%$ ) and high variability ( $CV > 60\%$ ) [38].

Outliers were filtered out considering data below the lower limit (Li) or above the upper limit (Ls) as discrepant [39]. However, during the kriging process, outliers were also considered. Such points, although deviating from the mean, were deemed representative of actual field conditions, thereby enhancing the accuracy of the resulting maps.

For the geostatistical analysis, the GEOEAS geostatistical tool was used. The spatial dependence of salinity and sodicity was analyzed using the classic semivariogram constructed from the semivariance estimate given by Equation (4) [40].

$$\hat{\gamma}(h) = \frac{1}{2N(h)} \sum_{i=1}^n [Z(X_i + h) - Z(X_i)]^2 \quad (4)$$

where  $\hat{\gamma}(h)$  = estimated value of the semivariance of the experimental data;  $Z(X_i + h)$  and  $Z(X_i)$  = observed values of the regionalized variable; and  $N(h)$  = number of pairs of measured values, separated by a distance  $h$ .

With the experimental semivariogram in hand, the exponential, gaussian and spherical models were tested. The mathematical adjustment made it possible to define the following parameters: nugget effect (C0), range (A) and sill (C1).

The model that presented the best fit to the experimental values was chosen, according to the leave-one-out cross-validation technique [41], in which each of the measured values is interpolated by the kriging method, and the measured values are then replaced by the estimated and then calculated the distribution of standardized errors, which should present a mean close to zero and standard deviation close to one [40]. This method provides reliable and unbiased estimates of model efficiency.

The spatial dependence index (SDI) was calculated as the ratio between the nugget effect and the sill of theoretical semivariograms [42]. This criterion establishes a strong dependence when a given ratio is less than 25%, moderate for a ratio between 25 and 75%, and weak when the ratio is greater than 75%.

After validating the semivariogram, universal kriging of the data was applied and spatial distribution maps were created using the Surfer for Windows software, version 8.0 [43]. Kriging provides unbiased spatial predictions and quantify estimation errors through the kriging variance and reproduces the actual values at the measured points. This feature makes it particularly suited for assessing groundwater quality indicators, as it accounts for spatial dependence in the dataset [6,30]. However, kriging assumes a stationary mean and variance within the study area, which may not fully capture local variations in highly heterogeneous environments like Mimoso Alluvial Valley.

### 2.5. Sequential Gaussian Simulation

The sequential Gaussian simulation (SGS) method was applied to the groundwater quality for the irrigation indicator (GWQ), generating simulated values at each location based on a conditional cumulative distribution function (CCDF) estimated at each step. To perform SGS, the original data needed to be transformed into a gaussian distribution. This transformation was achieved by converting the normal score [25]. This approach was selected to complement kriging by providing a probabilistic framework that better represents spatial uncertainty and preserves natural variability, particularly in areas with sparse data.

The CCDF used in SGS relies on the mean and covariance structure of the dataset, assuming a random gaussian field. By repeatedly running these sequential steps with varying random paths, different spatial distribution realizations are generated. The SGS algorithm was run 100 times to generate multiple realizations, ensuring robust probability calculations and variability representation [24]. This method addresses limitations of kriging, that lead to a smoothing effect, resulting in an overestimation or underestimation of values, thereby restricting its applicability to assess uncertainties for some situations. Nevertheless, SGS requires careful parameterization, including semivariogram modeling and normal score transformation. The implementation was conducted using GS+ software (version 7.0).

### 2.6. Multivariate Analysis

Principal Component Analysis (PCA) was conducted using the Comprehensive R Archive Network (CRAN) package in R programming to determine the key variables, such as rainfall, evapotranspiration and groundwater abstraction, that significantly influence the dynamics of groundwater salinity and sodicity.

## 3. Results and Discussion

### 3.1. Climatic Dynamic

The time series of monthly precipitation and evapotranspiration for the year 2019 are presented in Figure 3. Average monthly precipitation was higher than normal in March, July, and December, and lower than usual for all other months. Evapotranspiration values generally stayed within the historical average range but showed more fluctuation from May to August due to the increased rainfall and lower air temperatures. The average groundwater exploitation rates corresponded inversely to the water availability from precipitation, showing high values from October to December, with a peak in 2019 for October, which is typically a low-rainfall month in the region. It is observed that after the rainy period of June and July, the month of August already had a significant exploitation rate, despite the low precipitation index.

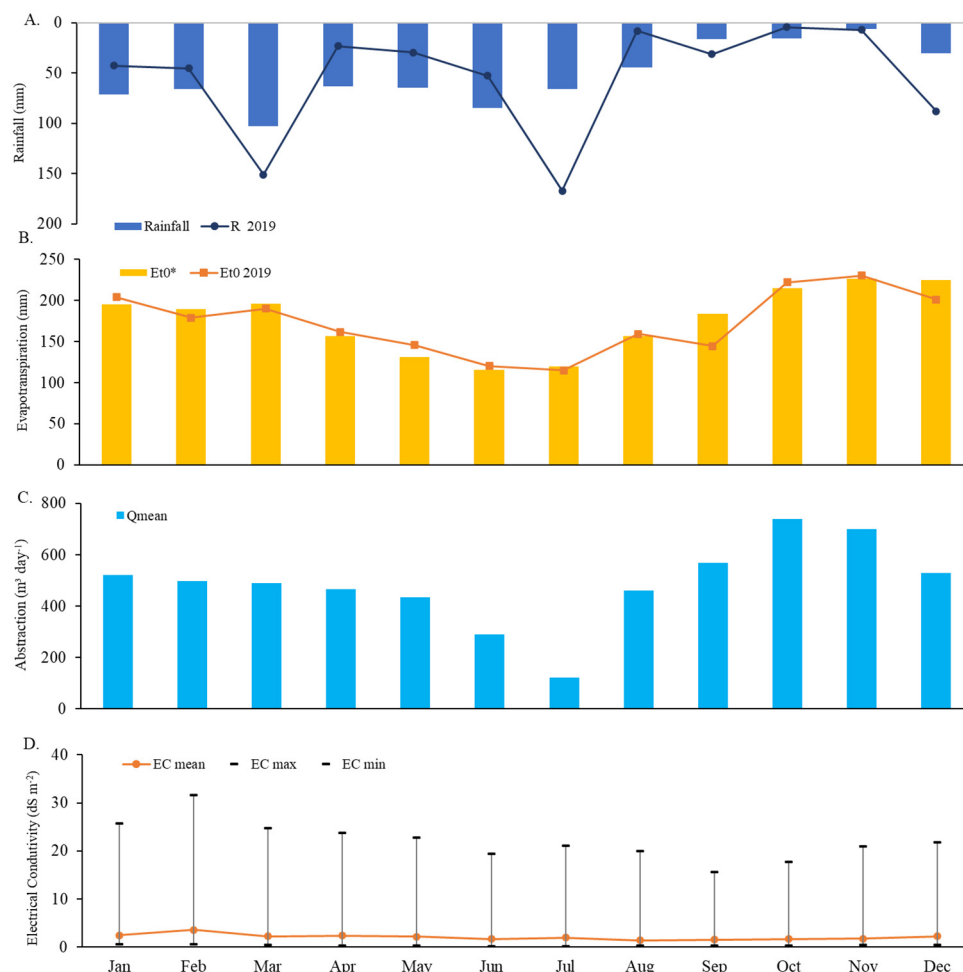


**Figure 3.** Historical monthly averages and 2019 data for meteorological parameters as rainfall (A), water exploitation averages (B), and the maximum, minimum, and mean EC values for 2019 (C). (R = accumulated rainfall; Rainfall = historical average rainfall of 20 years; Et0 = reference evapotranspiration; Et0\* = historical average evapotranspiration; Qmean = daily exploitation per month; ECmean = mean electrical conductivity; ECmin = minimum electrical conductivity; (D) ECmax = maximum electrical conductivity).

The electrical conductivity (EC) values ranged from 0.35 to 25.79 dS m<sup>-1</sup>, with standard deviations of 3.04 to 7.3, indicating a high degree of variation from the mean. This was supported by high values of coefficients of variation ( $\leq 1.94$ ). Extreme values in datasets of Mimoso Alluvial Valley were observed over three consecutive years (2007, 2008 and 2009) [10]. Altogether, nine piezometers exhibited extremely high EC readings throughout the year, with three of them showing extremely high values in every monitored month. These values were initially filtered out for the estimation of the mean semivariogram. By excluding these outliers, the dataset achieved a more balanced representation of the central tendency and dispersion, facilitating a more accurate geostatistical analysis while still capturing the overall variability of EC and the SAR in the study area. However, for the kriging interpolation, the outlier data were reintroduced. Despite their divergence from the overall dataset mean, these values were retained to ensure the mapping accurately reflecting the actual field conditions. Their inclusion acknowledges the existence of specific areas with significantly higher salinity, which are critical for understanding the spatial variability and potential management implications. These nine piezometers, which were excluded from the initial analysis, were located in the longitudinal region of the valley [6,44]. This area has a greater accumulation of salt due to the confluence of the Ipaneminha and

Mimoso streams and is characterized by a high concentration of salts in both the soil and the groundwater.

Filtered data were employed to compute the mean semivariogram within the study area. The coefficient of variation for electrical conductivity (EC), after the exclusion of outliers, exhibited a range of 30–40%, categorizing it as displaying moderate variation. This adjustment reflects a reduction in variability compared to the unfiltered data, which initially showed a high coefficient of variation. This data normalization procedure proved successful, with the Kolmogorov–Smirnov test at a 5% significance level yielding Dn (max) values of 0.13, 0.08, 0.13, 0.08, 0.21, 0.15, 0.18, 0.14, 0.21, 0.08, 0.15, 0.21 and corresponding *p*-values of 0.48, 0.96, 0.65, 0.99, 0.13, 0.20, 0.19, 0.41, 0.40, 0.12, 0.17, and 0.22 for the months spanning from January to December, respectively.

### 3.2. Groundwater Quality

Statistics for major ions and SAR data in 2019 are listed in Table 2. Based on the mean values the order of these cations is  $\text{Ca}^{2+} > \text{Mg}^{2+} > \text{Na}^+ > \text{K}^+$ . There was a wide range of variation for all ions throughout all months, with  $\text{Na}^+$ ,  $\text{Ca}^{2+}$ , and  $\text{Mg}^{2+}$  exhibiting the most variability. The average concentrations of  $\text{Ca}^{2+}$ ,  $\text{Mg}^{2+}$ ,  $\text{Na}^+$ , and  $\text{K}^+$  were 38.4%, 38.3%, 13.8%, and 9.4%, respectively, calculated based on their eight concentrations.

**Table 2.** Monthly descriptive statistics of groundwater chemical parameters in Mimoso Alluvial Valley.

	May	Jun	Jul	Aug	Sep	Oct	Nov
<b>A. Sodium (<math>\text{mg L}^{-1}</math>)</b>							
Number of Samples	41	40	38	40	41	40	41
Mean	125	114.4	91.5	93.3	118.5	126.5	118.2
Maximum	595.2	609.7	609.7	541.8	554.5	555.4	577.5
Minimum	44.3	11	8.3	46.9	61.2	60.3	53.7
Standard Deviation	133.8	114.2	108.1	90.1	103.9	117.2	104.4
Coefficient of Variation	1.07	1	1.18	0.97	0.88	0.93	0.88
<b>B. Potassium (<math>\text{mg L}^{-1}</math>)</b>							
Mean	68.7	79	75.9	74.3	85.5	74.6	74.8
Maximum	95.1	110.3	110.3	108.9	113.5	95.1	108.9
Minimum	15.6	1.1	15.6	30	37.4	41.6	33.7
Standard Deviation	20.2	25	23.2	19.7	20.5	15.7	21.9
Coefficient of Variation	0.29	0.32	0.31	0.27	0.24	0.21	0.29
<b>C. Calcium (<math>\text{mg L}^{-1}</math>)</b>							
Mean	332.9	262.2	242.9	347.4	338.3	374.4	278.6
Maximum	2905.8	1282.6	721.4	1082.2	1683.4	1683.4	1603.2
Minimum	80.2	48.1	60.1	100.2	120.2	80.2	56.1
Standard Deviation	459.6	223.2	160.8	218.9	305	388.2	308.7
Coefficient of Variation	1.38	0.85	0.66	0.63	0.9	1.04	1.11
<b>D. Magnesium (<math>\text{mg L}^{-1}</math>)</b>							
Mean	294.4	284.7	260.8	217.6	410.2	309.6	394.3
Maximum	1507.2	1653.1	1337.1	875.2	2042	1416.1	2066.4
Minimum	12.2	24.3	24.3	24.3	24.3	36.5	24.3
Standard Deviation	347	276.6	252.6	188	509	279.9	415.9
Coefficient of Variation	1.18	0.97	0.97	0.86	1.24	0.9	1.05
<b>E. Total Hardness (<math>\text{mmol L}^{-1}</math>)<sup>0.5</sup></b>							
Mean	90.8	86.9	84.1	85.2	100.6	94.2	96.4
Maximum	278	250	168.0	160.0	236.1	176.0	260.0
Minimum	60	66	66.0	68.0	60.0	68.0	68.0
Standard Deviation	43.6	30.9	21.4	17.9	42.9	28.0	42.8
Coefficient of Variation	47.9	35.5	25.4	21.0	42.6	29.8	44.4

Table 2. Cont.

	May	Jun	Jul	Aug	Sep	Oct	Nov
F. Sodium Adsorption Ratio ( $\text{mmol L}^{-1}$ ) <sup>0.5</sup>							
Mean	6.7	6.7	5.8	5.3	7	7	6.5
Maximum	19.4	22.5	35.1	18.9	30.5	22	15.4
Minimum	3	0.8	0.4	3.3	2.5	2.7	2.9
Standard Deviation	3.6	3.6	6	2.8	6	4.7	2.7
Coefficient of Variation	0.54	0.54	1.03	0.53	0.86	0.67	0.42
G. Electrical Conductivity ( $\text{dS m}^{-1}$ )							
Mean	1.67	1.41	1.45	0.79	1.26	1.39	1.43
Maximum	18.43	19.37	19.37	1.60	15.00	16.65	20.90
Minimum	0.35	0.25	0.26	0.34	0.39	0.35	0.51
Standard Deviation	3.57	3.15	3.23	0.30	2.22	2.54	3.04
Coefficient of Variation	2.13	2.24	2.22	0.38	1.76	1.82	2.13

The  $\text{Ca}^{2+}/\text{Mg}^{2+}$  is also a key indicator of water hardness, which is an important hydrogeochemical indicator of water composition, as it reflects the dissolution of silicate minerals within the water. In the present study, this ratio was approximately 1, indicating that dolomite from the lens rock is undergoing dissolution [45]. The average values of total hardness for May, June, July, August, October and November were recorded as 90.8; 86.9; 84.1; 85.2; 100.6; 94.2 and 96.4 ( $\text{mmol L}^{-1}$ )<sup>0.5</sup>, respectively, indicating that the water was classified as ranging from moderate to hard throughout all months. Similar values were found in southwestern Nigeria and concluded that values below  $600 \text{ mg L}^{-1}$  are not considered to pose any environmental risks and are safe to use [46]. The main factors responsible for the enrichment of groundwater with magnesium and calcium are  $\text{Ca}^{2+}$ – $\text{Mg}^{2+}$  exchanges stemming from the interaction between water and carbonates present in the rock, as well as ionic exchanges between  $\text{Ca}^{2+}$ ,  $\text{Mg}^{2+}$  and  $\text{Na}^+$  [47].

$\text{Na}^+$  and  $\text{K}^+$  concentrations ranged from 8.3 to  $609.7 \text{ mg L}^{-1}$  and from 1.1 to  $113.5 \text{ mg L}^{-1}$ , respectively, showing high and medium variability. The groundwater K contents were in general low, with a high concentration in places where fertilizers in the form of potassium sulfate, potassium chloride or potassium nitrate are used in agricultural activities [48].

The relationship between the  $\text{Na}^+$  content and other cations was expressed as the percentage of sodium (PS). The average percentages for May, June, July, August, October, and November were 17.9%, 18.2%, 15.7%, 14.6%, 14.2%, 16.7%, and 15.8%, respectively. The results do not indicate sodium-related issues; however, three monitoring points consistently showed elevated percentages ranging from 60% to 72% during the evaluated months. Similar findings were reported when assessing the spatial variation in water quality in the Doukkala plain, Morocco, that irrigation with water carrying a sodium percentage exceeding 60% could result in sodium accumulation in the soil, potentially leading to soil structure degradation [3].

The sodium adsorption rate (SAR), ranged from 0.8 to 35.1 ( $\text{mmolc L}^{-1}$ )<sup>0.5</sup>, being classified as moderate to strong. The correlation values between ions can be used to determine the origin of ions in groundwater, where the increase or decrease in ions in groundwater is used as an indication of mineral dissolution [14]. Spearman's correlation between salt contents, EC and the SAR for May to November 2019 can be seen in Table 3.

**Table 3.** Spearman’s correlation between salt contents, electrical conductivity (EC) and the sodium adsorption ratio (SAR) from May to November 2019.

A. May								B. June							
	EC	Na <sup>+</sup>	K <sup>+</sup>	Ca <sup>2+</sup>	Mg <sup>2+</sup>	SAR	R		EC	Na <sup>+</sup>	K <sup>+</sup>	Ca <sup>2+</sup>	Mg <sup>2+</sup>	SAR	R
EC	1.00							EC	1.00						
Na	−0.10	1.00						Na	0.44	1.00					
K	−0.48	0.38	1.00					K	−0.25	−0.22	1.00				
Ca	−0.07	0.65	0.31	1.00				Ca	0.49	0.58	0.08	1.00			
Mg	−0.01	0.93	0.42	0.46	1.00			Mg	0.58	0.84	−0.12	0.58	1.00		
SAR	0.67	−0.15	−0.43	−0.04	−0.07	1.00		SAR	0.72	0.17	−0.24	0.10	0.25	1.00	
R	−0.06	0.31	−0.09	0.15	0.21	−0.04	1.00	R	−0.11	0.05	0.12	0.01	0.10	−0.03	1.00
C. July								D. August							
	EC	Na <sup>+</sup>	K <sup>+</sup>	Ca <sup>2+</sup>	Mg <sup>2+</sup>	SAR	R		EC	Na <sup>+</sup>	K <sup>+</sup>	Ca <sup>2+</sup>	Mg <sup>2+</sup>	SAR	R
EC	1.00							EC	1.00						
Na	−0.06	1.00						Na	−0.15	1.00					
K	−0.16	0.32	1.00					K	−0.17	−0.12	1.00				
Ca	−0.07	0.39	0.29	1.00				Ca	0.46	0.11	−0.21	1.00			
Mg	−0.05	0.77	0.32	−0.11	1.00			Mg	−0.20	0.18	−0.10	−0.15	1.00		
SAR	0.91	−0.11	−0.14	−0.04	−0.14	1.00		SAR	−0.03	−0.12	0.26	−0.21	0.20	1.00	
R	0.20	−0.10	−0.34	0.07	−0.20	0.15	1.00	R	0.02	−0.21	−0.12	0.11	0.24	−0.04	1.00
E. September								F. October							
	EC	Na <sup>+</sup>	K <sup>+</sup>	Ca <sup>2+</sup>	Mg <sup>2+</sup>	SAR	R		EC	Na <sup>+</sup>	K <sup>+</sup>	Ca <sup>2+</sup>	Mg <sup>2+</sup>	SAR	R
EC	1.00							EC	1.00						
Na	−0.13	1.00						Na	−0.19	1.00					
K	−0.22	0.38	1.00					K	0.13	−0.16	1.00				
Ca	−0.16	0.25	0.30	1.00				Ca	0.07	0.44	−0.06	1.00			
Mg	−0.14	−0.19	−0.44	−0.09	1.00			Mg	−0.13	0.19	−0.12	−0.17	1.00		
SAR	0.93	0.02	−0.09	−0.15	−0.21	1.00		SAR	0.68	−0.24	0.18	−0.16	0.02	1.00	
R	−0.05	−0.09	0.05	−0.16	−0.07	−0.04	1.00	R	−0.08	−0.10	0.17	−0.12	0.04	−0.11	1.00
G. November															
	EC	Na <sup>+</sup>	K <sup>+</sup>	Ca <sup>2+</sup>	Mg <sup>2+</sup>	SAR	R								
EC	1.00														
Na	−0.14	1.00													
K	−0.02	0.25	1.00												
Ca	0.02	0.90	0.45	1.00											
Mg	−0.20	0.50	0.06	0.42	1.00										
SAR	0.83	−0.17	0.18	−0.03	−0.27	1.00									
R	−0.08	0.80	0.34	0.82	0.43	−0.09	1.00								

The correlation matrix showed positive and statistically significant correlations between the SAR and EC, as well as positive relationships among most analyzed cations over the months. An exception was observed in August, where the SAR × EC correlation was negative and non-significant. This result can be explained by analyzing the interplay between climatic factors, reflecting the combined effects of low rainfall, high evapotranspi-

ration, and anthropogenic factors, such as intensive irrigation and fertilizer application. In August, as can be seen in Figure 2, accumulated precipitation ( $R = 7.8$  mm) is low, while evapotranspiration ( $ET_0 = 159.2$  mm) remained close to the historical average of 156.3 mm. These conditions are characteristic of the beginning of the dry season, where minimum precipitation and high evaporative demand reduce aquifer recharge and increase groundwater salt concentration due to evaporation. Despite the high mean electrical conductivity ( $EC_{mean} = 1.39$  dS  $m^{-1}$ ), the observed decrease in the SAR suggests a change in the ionic composition of the groundwater, specifically the relative concentrations of  $Ca^{2+}$  and  $Mg^{2+}$ .

This transition period between the wet and dry seasons typically represents a period of intensified irrigation to support crops. The application of irrigation water, often supplemented with fertilizers containing calcium or magnesium salts, may have disproportionately increased the concentrations of  $Ca^{2+}$  or  $Mg^{2+}$  in the groundwater. Furthermore, previous studies indicate that the region studied is influenced by regional underground flow and by contributions from runoff from the valley slopes that feed the water table, even during the dry season, a fact that also contributes to the increase in salinity, both of the soil and of the water in the central region of the alluvial valley, since it carries part of the salts present in the soil from the weathered rocks at the hillslopes to this specific region of the valley [5,10].

### 3.3. Spatial Distribution Map of EC and the SAR

The semivariograms scaled by variance for electrical conductivity, from January to December 2019, are shown in Figure 4. The semivariograms were properly validated according to the leave-one-out cross-validation criterion with a standard deviation close to one (0.93; 1.10; 0.97; 0.92; 1.20; 0.98; 1.01; 1.09; 1.03; -0.86; 1.08; -0.95), as well as mean errors close to zero (0.04; 0.14; -0.02; -0.01; 0.05; -0.01; -0.02; -0.05; -0.04; -0.06; -0.01; 0.05), from January to December 2019, respectively.

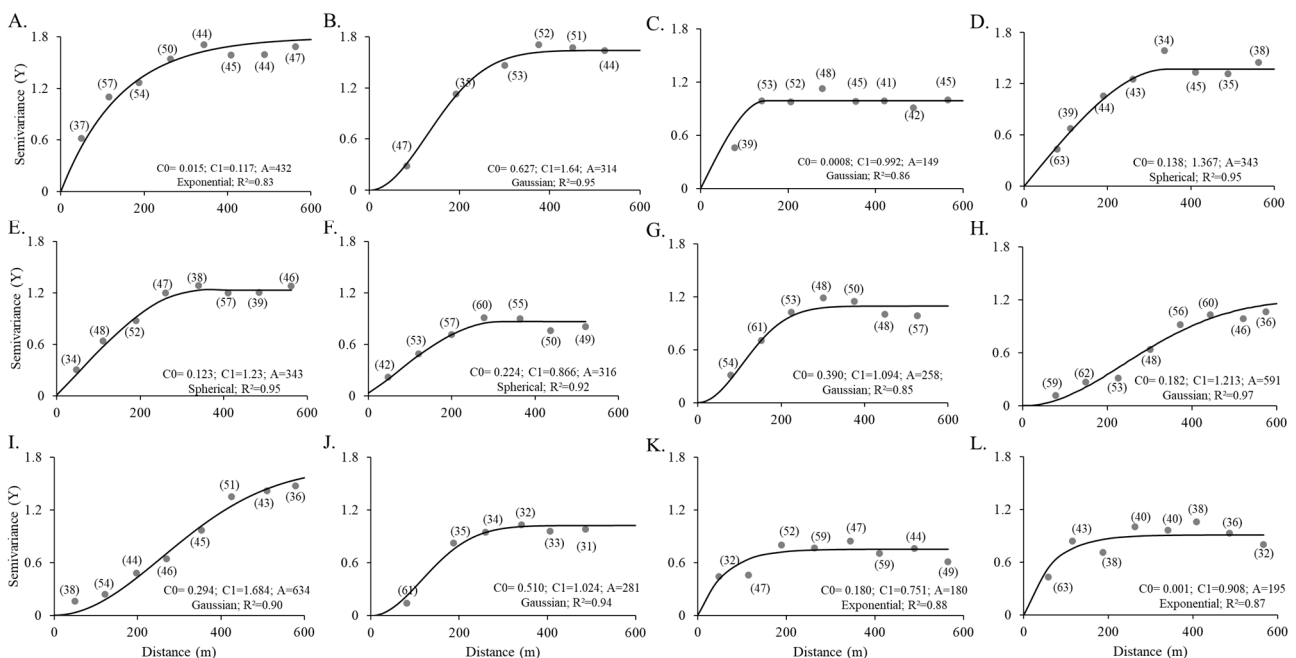


**Figure 4.** Semivariograms scaled by electrical conductivity variances and adjustments of the exponential, gaussian and spherical models, from January to December (A–L) 2019. C0 represents the nugget effect, C1 the sill, A the model range and R<sup>2</sup> the determination coefficient.

Electrical conductivity exhibits a spatial dependence structure in the studied area, with ranges varying from 180 to 634 m. Spatial dependence can be considered strong for

January, March, April, May, September, November, and December. For February, June, July, August, and October, dependence was considered moderate. In the present study, no clear dependence pattern was observed with respect to the dry and wet seasons, as indicated by non-significant correlation coefficients (Table 3) between precipitation and EC. This phenomenon can be attributed to water abstraction for agricultural activities in the region, which disrupts the aquifer’s recharge process and, as a result, alters the dynamics of salt dilution within the system.

Regarding the SAR, gaussian, spherical, and exponential models were fitted, as shown in Figure 5. Semivariograms were properly validated using leave-one-out cross-validation criteria, with standard deviations close to one (1.02, 1.14, 1.09, 1.11, 1.04, 1.02, 1.30) and mean errors close to zero (−0.002, −0.003, 0.010, −0.003, −0.030, 0.128, 0.020).

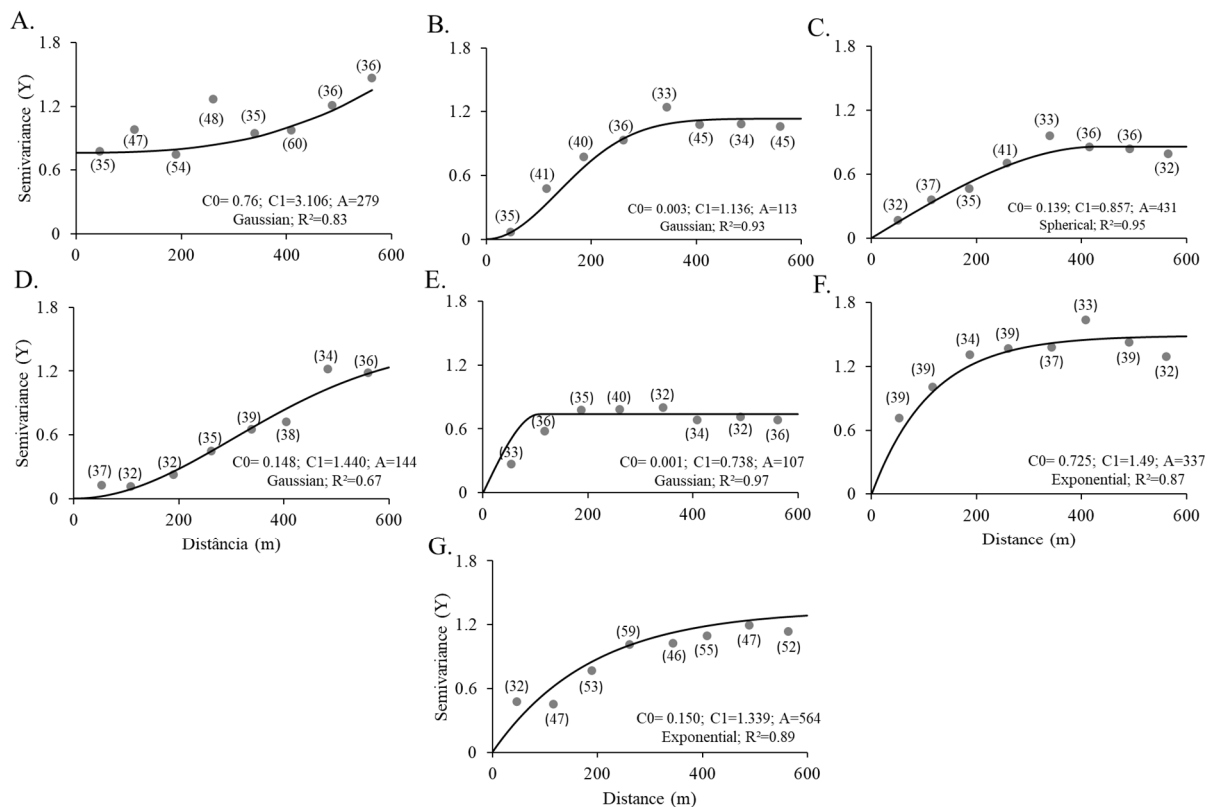


**Figure 5.** Semivariograms scaled by the SAR variances and adjustments of the exponential, gaussian and spherical models, from May to November (A–G) 2019. C0 represents the nugget effect, C1 the sill, A the model range and  $R^2$  the determination coefficient.

The ranges varied from 107 to 564 m, exhibiting strong spatial dependence over the months, except for October, which showed moderate dependence. It was also not possible to associate the model changes with a specific rainfall variation pattern.

In Figure 6, the crossed semivariograms are visualized for the SAR and EC, from May to November 2019, in order to assess the co-regionalization between them. All fitted semivariogram models were adjusted and properly validated according to the leave-one-out cross-validation criterion. The spherical, gaussian and exponential models presented standard deviation close to one (0.97; 1.01; 0.89; 0.99; 1.04; 0.95; 1.11), as well as the mean errors close to zero (−0.06; 0.10; −0.02; −0.02; 0.02; −0.01; −0.02).

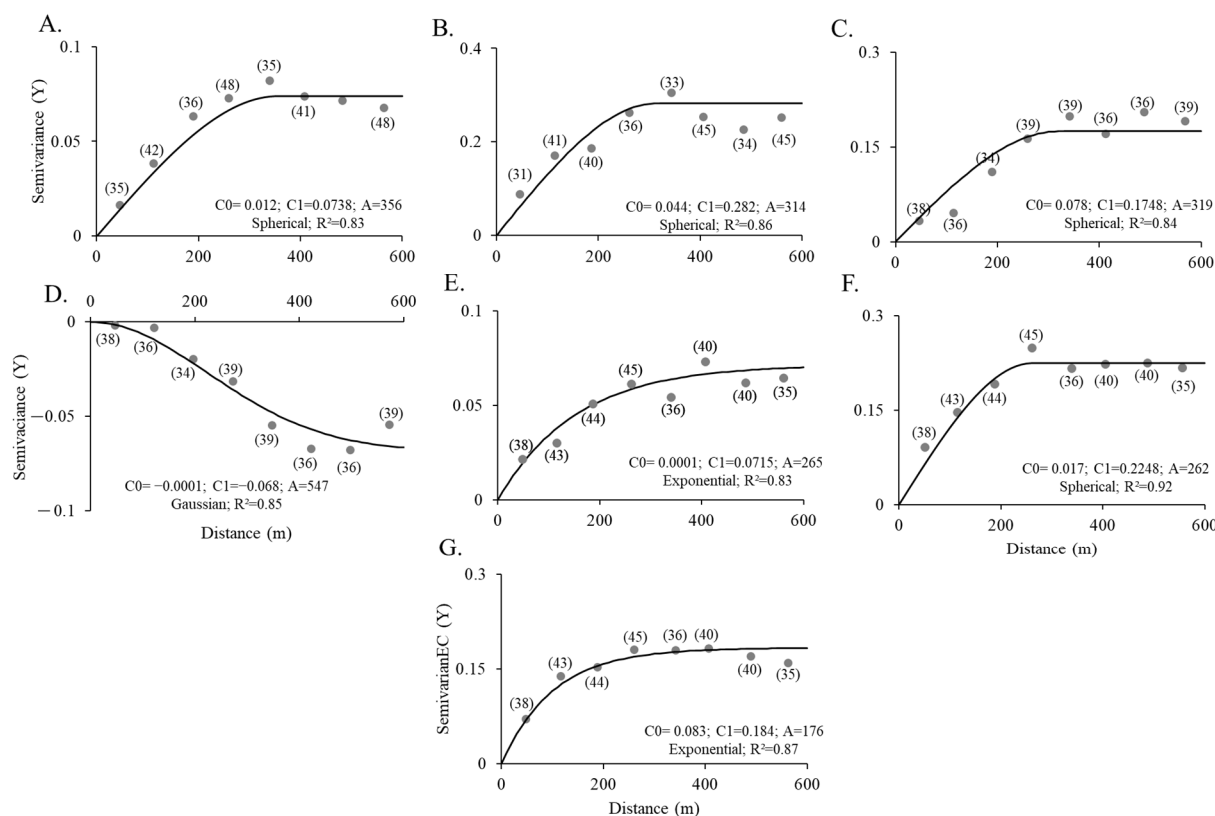


**Figure 6.** Crossed semivariograms of the SAR  $\times$  CE and adjustments of the exponential, gaussian and spherical models, from May to November (A–G) 2019. C0 represents the nugget effect, C1 the sill, A the model range and  $R^2$  the determination coefficient.

The crossed semivariograms indicated a strong correlation between the variables with determination coefficients ( $R^2$ ) greater than 80%. Experimental semivariances were obtained considering at least 30 pair of points [40]. The identification of highly representative models for the spatial behavior of the SAR and EC demonstrates the spatial correlation and interdependence between these variables. In this context, combining both to determine a water suitability class for agricultural purposes is well-founded and consistent, enabling a more comprehensive and accurate assessment of water quality, which is essential for sustainable management in vulnerable regions.

Ranges varied between 176 and 365 m, with moderate to strong spatial dependence. For August, a negative correlation was observed, that is, the effects of increasing the sodium adsorption ratio increased as the water salinity decreased. This behavior can be attributed to the use of soil for agricultural purposes [48] and the consequent application of fertilizers, which promote an ionic imbalance in the aquifer. Additionally, low salinity levels are often associated with reduced concentrations of calcium and magnesium as water hardness is the main contributor to salinity in the MAV region. This imbalance, combined with the use of fertilizers, leads to an increase in the relative proportion of sodium ions and, consequently, a higher SAR [49].

The adjusted models were used to create isoline maps of electrical conductivity, as shown in Figure 7, using the kriging technique. According to Richards' classification [36], the groundwater samples showed varying salinity levels throughout the year. Low salinity was observed in 14% to 52% of the samples, with the highest percentages occurring from September to October. Moderate salinity predominated, ranging from 37% to 77%, while high salinity was less frequent, appearing in 3% to 18% of the samples, with lower values generally observed in the second half of the year.

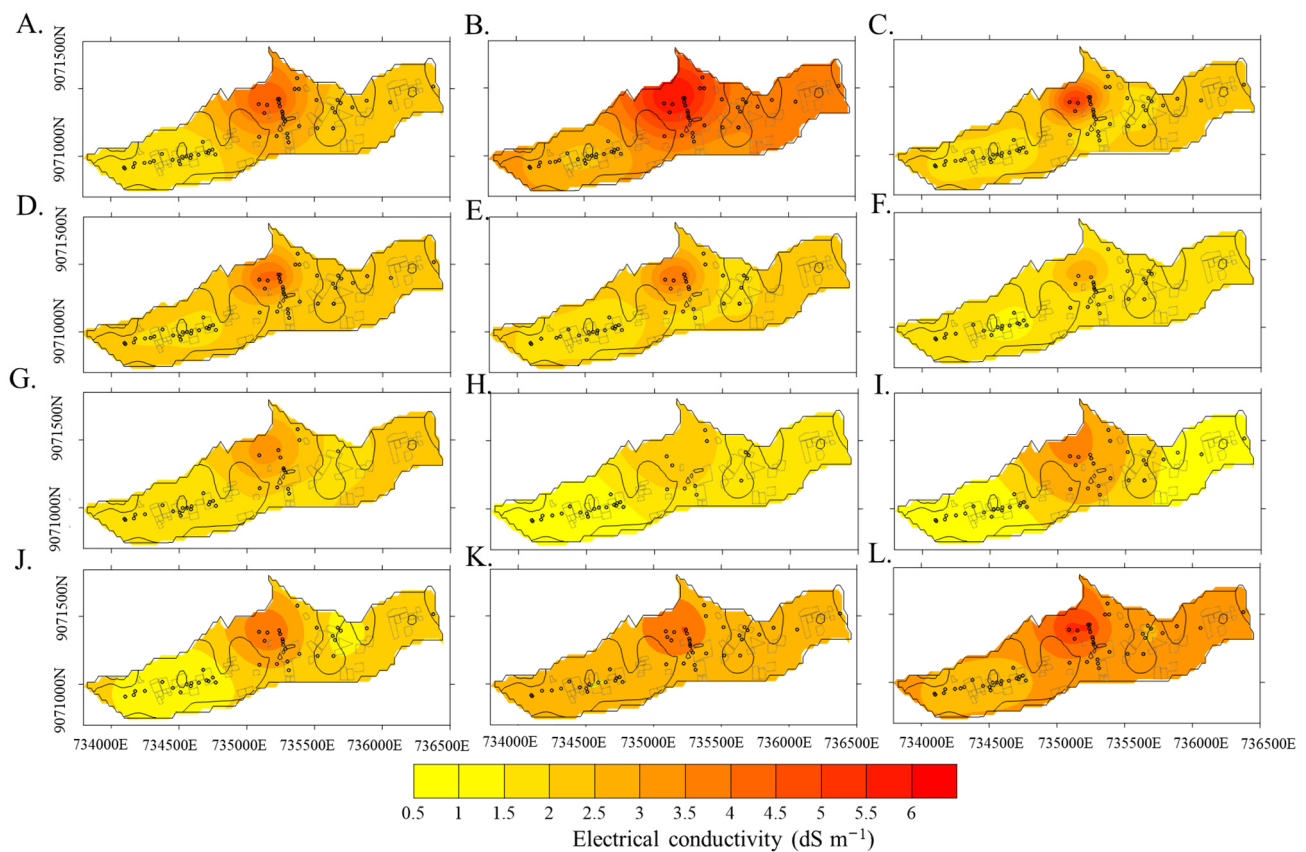


**Figure 7.** Electrical conductivity (EC) kriging maps from January to December (A–L) 2019 with agricultural plots and saturated electrical conductivity contours.

The regions with the highest EC are located at the boundaries of the valley, where soil texture is finer, and the impediment layer (e.g., hard-rock granite complex basement) is closer to the soil surface, hence with lower aquifer thickness [4,10]. Previous studies indicated that this region is influenced by the regional underground flow and by contributions of lateral flow and groundwater flow through the upper fissured layer from the slopes of the valley that feed the water table, which also favors the increase in salinity, since it carries part of the salts present in the soil of the hillslopes for this region, and the dissolution of salts from the saprolite zone [5,44].

It was observed that the electrical conductivities that presented values lower than  $4 \text{ dS m}^{-1}$  were highly influenced by diffuse recharge from precipitation. Areas that had groundwater with electrical conductivity above this value tended not to suffer variations, maintaining high concentrations over time. This stability in salinity suggests a persistent risk of soil salinization and reduced crop productivity, emphasizing the importance of proactive management strategies. Note that in February (Figure 5B) there were higher EC values in the western region, to the detriment of the leaching of salts from the soil profile into the aquifer. In August, on the other hand, had the lowest concentration of salts in the water due to the rainfall events accumulated over the months. In September, there is a new dynamic of salt concentration in the water, due to greater evapotranspiration and constant water withdrawals, which increase in this period.

The spatiotemporal dynamics of the sodium adsorption ratio is shown in the kriging maps in Figure 8.

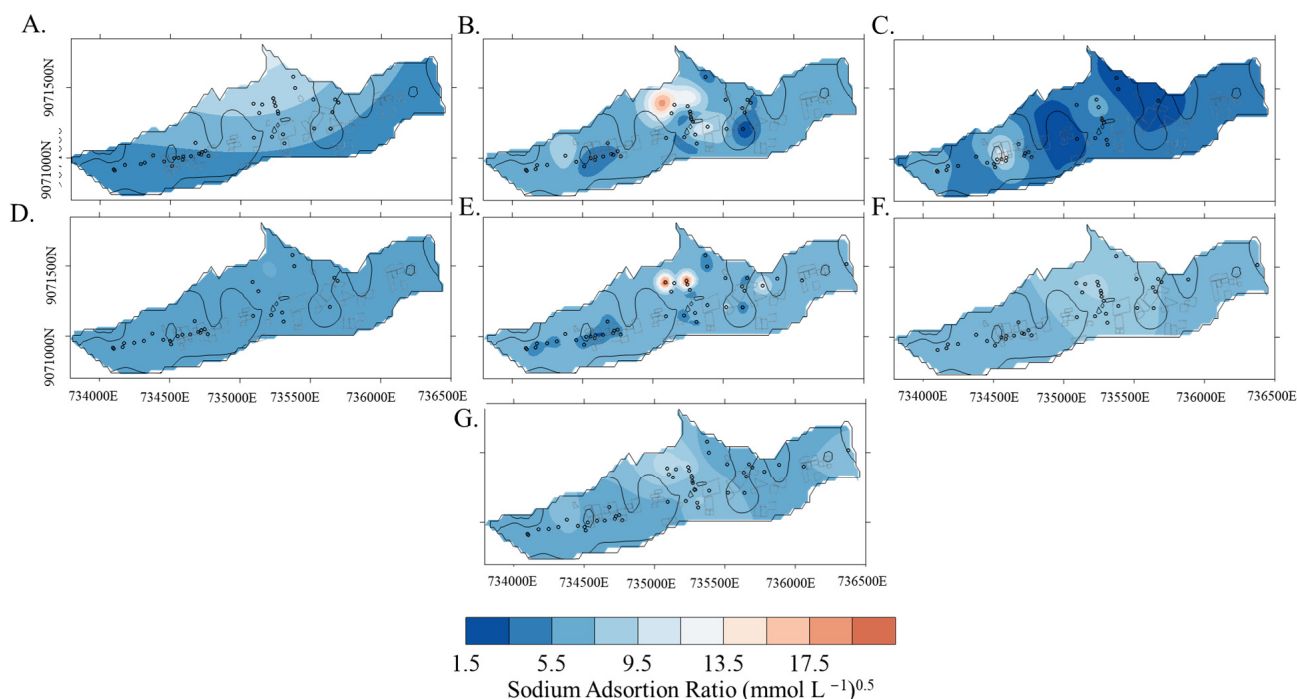


**Figure 8.** Sodium adsorption ratio (SAR) kriging maps from May to November (A–G) from 2019, with agricultural plots and saturated electrical conductivity contours.

The SAR spatial distribution shows that the highest values represented a moderate risk [36] and mostly present spatiotemporal dynamics similar to those of electrical conductivity, being directly proportional. However, the presence of high levels of sodium for June, July and November in the western portion of the valley stands out. June and July tend to exhibit the highest electrical conductivities, a behavior likely attributed to the leaching of salts from the unsaturated zone due to the accumulated rainfall during the rainy season in the valley [10]. Additionally, an increase in salt concentrations in groundwater is observed with the intensification of water scarcity, driven by the rise in evapotranspiration, which peaks in November. This indicates that groundwater salinization and degradation may be occurring [4]. Furthermore, the presence of agricultural plots in the area indicates that these results may be partially attributed to agricultural practices, such as the use of fertilizers and pesticides, which can exacerbate salinity levels [14].

### 3.4. Groundwater Quality Map for Irrigation Use

The spatial dynamics regarding electrical conductivity and the sodium adsorption ratio, which can be used to determine the suitability of groundwater for irrigation purposes, suggesting that more salinity tolerant crops could be cultivated with a good installation of a drainage system to mitigate the effects of soil salinization and improve agricultural production [20,50]. Mainly at those critical areas, organic fertilizers are recommended, along with the use of organic mulching on the soil surface of the irrigated plots, at the cultivation lines. Figure 9 presents the semivariograms of groundwater adequacy indicators, with adjustments to exponential, Gaussian, and spherical models for the months of May (A) through November (G) 2019.

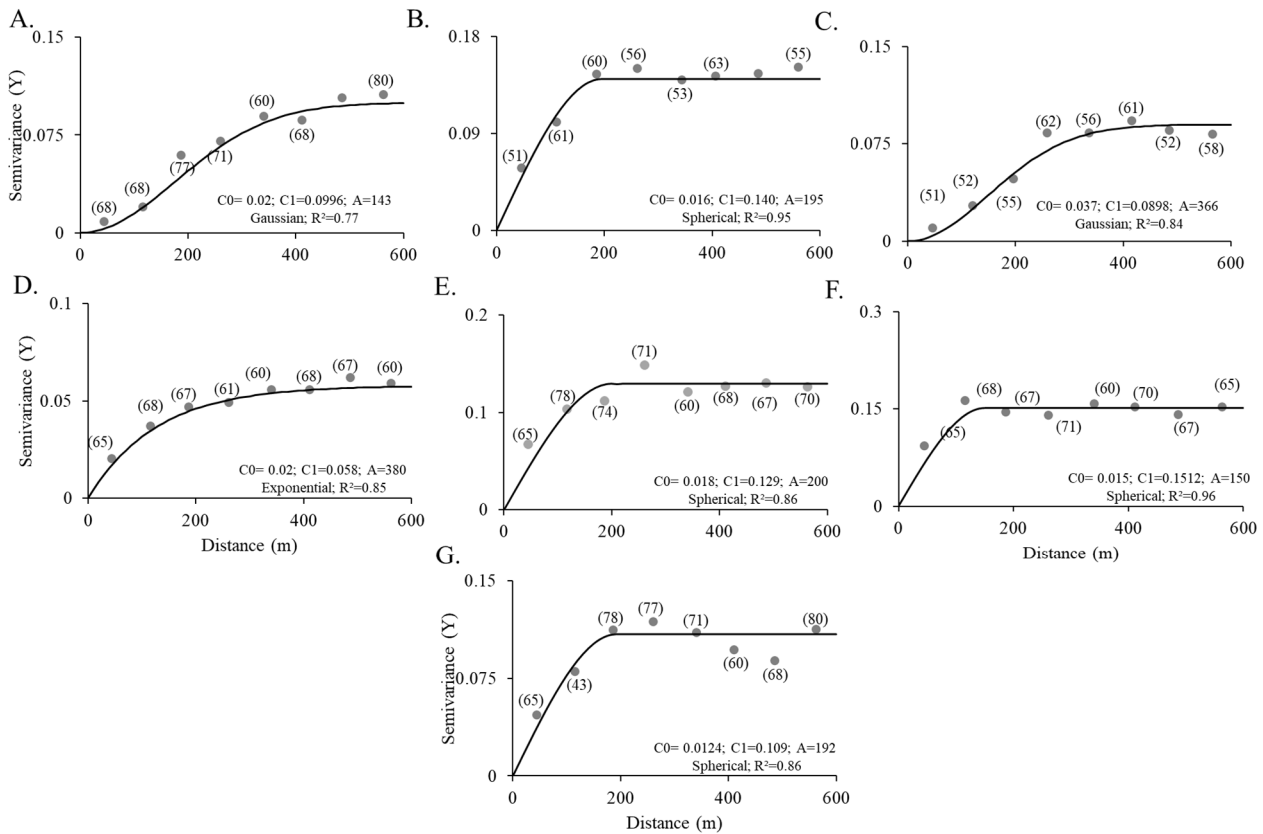


**Figure 9.** Semivariograms of the groundwater adequacy indicators and adjustments of the exponential, gaussian and spherical models, from May to November (A–G) 2019.

The results reveal distinct spatial dependency patterns across the monitoring period, with noticeable variations in model fit and range of spatial influence. A general pattern is observed where the spherical and Gaussian models demonstrate superior fit (higher  $R^2$  values) compared to the exponential model in most months. This suggests that the spatial structure of groundwater quality indicators tends to stabilize over short to moderate distances. For instance, the Gaussian model dominates in May (A) and July (C), while the spherical model exhibits the best fit in November (G), indicating seasonal variations in spatial behavior.

The gaussian, spherical and exponential models presented standard deviation close to one (1.02; 1.10; 1.09; 0.97; 0.98; 0.91; 1.11), as well as the mean errors close to zero (−0.10; 0.09; 0.08; 0.20; −0.05; −0.10; 0.07). The crossed semivariograms indicated a strong to moderate correlation with determination coefficients ( $R^2$ ) greater than 70%. Experimental semivariograms were obtained considering at least 50 pair of points [40].

The water quality indicator presents a structure of spatial dependence in the studied area with range values, representing the extent of spatial correlation, varying significantly, ranging from approximately 143 m in May (A) to 380 m in August (D). This variability highlights changes in the spatial continuity of groundwater quality, likely driven by temporal factors such as recharge events, agricultural activities, and climatic conditions. The relationship between the nugget effect and the sill of semivariograms ranged from 10.0 to 41.2%; therefore, the spatial dependence can be considered from strong to moderate, over the months, with behavior very similar to that of EC. Overall, the results indicate a clear seasonal influence on the spatial dependency of groundwater adequacy indicators. While some months (e.g., May and November) exhibit strong spatial continuity, others (e.g., August) show a broader range, reflecting changes in environmental and anthropogenic influences. These

patterns underscore the need for continuous monitoring to account for both spatial and temporal variability in groundwater quality.

The fitted models were used to create contour maps of groundwater quality for irrigation purposes. In this map (Figure 10), areas suitable for irrigation are designated in green and blue, restricted use in yellow, while unsuitable areas are marked in red.

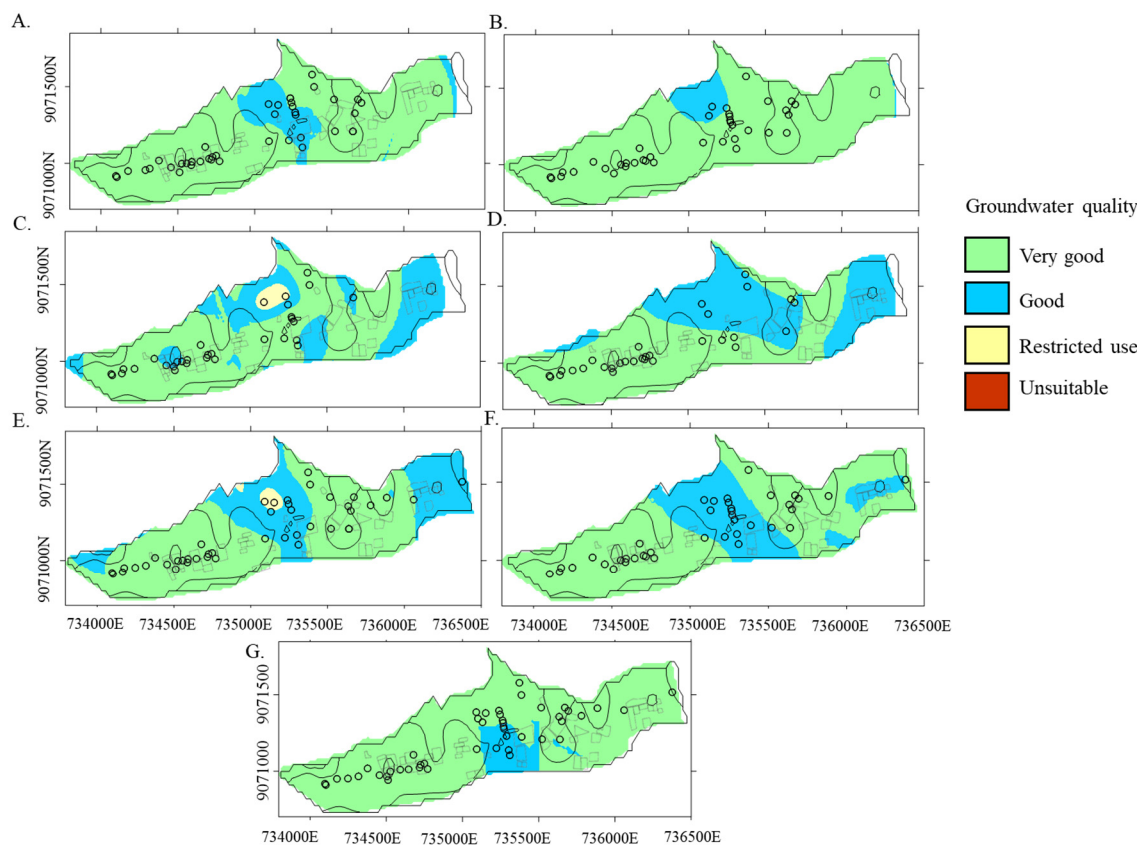


**Figure 10.** Kriging maps of groundwater quality for irrigation purposes from May to November (A–G) 2019, with agricultural plots and saturated electrical conductivity contours.

According to the maps, the most suitable areas for irrigation based on the water quality index are located in the western and eastern parts of the study area, with some exceptions in points where agriculture and exploitation activities are carried out more intensively. In these areas, high sodium concentration may reduce soil permeability and damage soil structure [51]. Only with mapping using kriging techniques was it not possible to detect areas where the water is classified as unsuitable for agricultural purposes.

Research on the characterization of spatial variability in groundwater parameters highlights the importance of conducting more comprehensive evaluations of uncertainty, particularly given the inherent heterogeneity of natural systems [17,18,27]. To address this, we performed conditional sequential Gaussian simulation to model the propagation of uncertainty for each sampling period, as illustrated in Figure 11. Data uncertainties can stem from potential measurement errors and the limited spatial coverage of field-collected samples [18]. Additionally, the variance of stochastic simulation is influenced by data values, with conditional variance being particularly significant when adjacent data points exhibit dissimilar values [52].

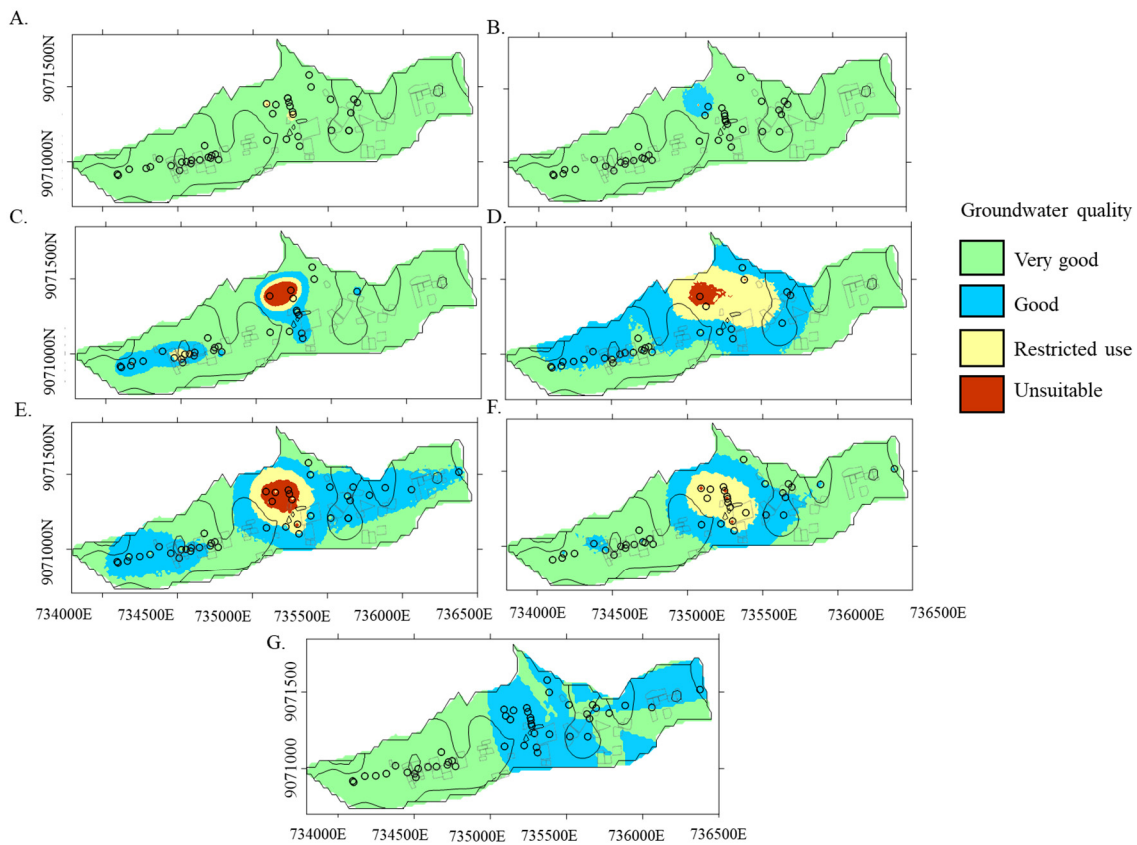


**Figure 11.** Sequential Gaussian simulation maps of groundwater quality for irrigation purposes from May to November (A–G) 2019 with agricultural plots and saturated electrical conductivity contours.

When comparing the scenario generated by the SGS with the kriging map, the large-scale variation remained conditioned, but the small-scale patterns exhibited differences, with the presence of water classes unsuitable for agricultural use that are sometimes represented by 4 or 5 points being smoothed by kriging. Moreover, by inspecting Figure 9 it is possible to verify that kriging was unable to reproduce the unsuitable class due to smoothing. Indeed, such areas are associated with low water circulation areas, exhibited in Figure 10. This behavior is expected, as the estimation of the local singularity exponent relates to all values within the neighborhood of the location being estimated [53]. Notably, there was a reduction in unsuitable areas for the month of July, while an increase was observed in the other evaluated months.

The updated spatial maps indicated that the percentage of unsuitable areas for irrigation ranged from 2.2% to 15.0% of the total area, while suitable areas comprised 67.0% to 97.8% during the assessed months. The identification of unsuitable areas underscores the need for targeted management strategies, such as the adoption of conservation practices, soil amendments, or crop selection tailored to saline conditions. These approaches could inform both local agricultural practices and policy interventions, ensuring long-term soil health and sustainable agricultural productivity in these vulnerable regions.

### 3.5. Interaction of Groundwater Quality and Climatic Conditions

To validate the results obtained in the previous analyses and illustrate the relationship between EC and the SAR with climatic parameters, soil hydraulics characteristics, as well as anthropogenic behavior related to water extraction for agricultural purposes, PCA was applied to the original matrix of electrical conductivity and the SAR. The PCA biplot for electrical conductivity is presented in Figure 12, along with their relationships with rainfall and water extraction for the evaluated months. It is observed that EC and the

SAR contribute significantly to the variability represented by Dim1 (dimension 1) (37.9%), indicating that these variables play a central role in the differences observed across the aquifer. Rainfall, on the other hand, is more closely associated with Dim2 (dimension 2) (19.5%), highlighting its impact through salinity dilution and ion transport. Soil texture (texture) appears as a moderating variable close to saturated hydraulic conductivity, uniformly distributed, while evaporation and water extraction (Q) are directly correlated with changes in EC and the SAR.

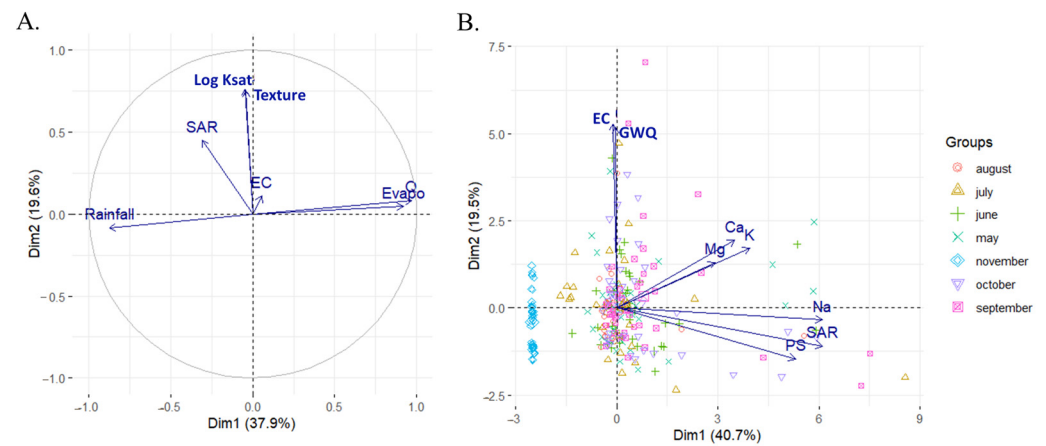


**Figure 12.** Principal Component Analysis (PCA) showing the scores of the first two principal components (A,B), which represent the directions of maximum variance in the dataset.

Additionally, the SAR and EC show a strong association with Dim1, along with Evapo, suggesting that evapotranspiration is one of the primary factors driving salinity increases. The PCA also highlights seasonal variations, which can be attributed to changes in precipitation and evapotranspiration patterns. The opposition between rainfall and variables such as the SAR, EC, and Evapo along Dim1 (37.9%) suggests an inverse relationship, where higher rainfall tends to dilute soil and water salinity. On the other hand, elevated evapotranspiration, aligned with EC and the SAR, indicates that increased evaporation can concentrate salts, leading to higher salinity levels, meaning that these variables play a central role in the differences observed in MAV dynamics.

In Figure 11B, the main components, Dim1 and Dim2, account for 60.2% of the total variance, with Dim1 alone explaining 40.7% of the data variability. For this component, samples from October and November exhibit greater variability, possibly due to reduced water recharge or intensive water use, whereas June and July show less variation. The variables Na, the SAR, and the PS form an associated group, highlighting the link between high sodium concentrations and the risks of soil sodicity, while  $\text{Ca}^{2+}$  and  $\text{Mg}^{2+}$  exhibit an opposing dynamic. Furthermore, salinity and the quality index (GWQ) are strongly associated with EC, which serves as the primary contributor to variations in water quality. These patterns support the hypothesis that seasonal and spatial factors, such as soil texture and effect of seasonality (e.g., rainfall and evapotranspiration dynamics), directly influence the suitability of water for agricultural use, with clear limitations in silty soil areas and during critical periods.

#### 4. Conclusions

This study provides critical insights into the suitability of groundwater in Mimoso Alluvial Valley for irrigation, emphasizing the spatial variability of water quality and its implications for agricultural practices. Moreover, the geostatistical analysis and the proposed quality index contributed to enhance the knowledge about the salinization

processes in alluvial valleys. To ensure sustainable agricultural use, the following findings and recommendations are highlighted:

1. The analysis of cations helped identify the natural salt dissolution process, originating from the crystalline rock in contact with aquifer-stored water. Targeted interventions, such as monitoring aquifer recharge areas, could mitigate further salinization.

2. Total hardness (TH) and Permeability Salinity (PS) analyses demonstrated that most of the alluvial valley is suitable for irrigation throughout the year in areas with high hydraulic conductivity. These areas should be prioritized for irrigation development.

3. Moderate to high salinity risk was observed in silt loam areas, requiring specific management practices to control salinity, as groundwater in these areas is unsuitable for sustainable irrigation.

4. Moderate sodicity risks were observed, with the highest risks concentrated in the central valley. Adaptive water management strategies, including seasonal adjustment of irrigation practices, are recommended to address temporal variability.

5. This study highlights the spatial variability of groundwater quality, identifying suitable irrigation areas and the implications of salinity using geostatistical maps. Sequential Gaussian simulation reduced mapping uncertainty, improving the accuracy of suitability assessments for irrigation.

6. The analysis of groundwater spatial variability, using advanced modeling techniques, revealed that unsuitable irrigation areas fluctuate throughout the year. Uncertainty simulations were essential for refining suitability estimates for irrigation.

7. The proposed water quality index successfully identified the more suitable regions for irrigation, being strongly related to EC and the SAR, as well as [Mg], and [Ca] concentrations. This index serves as a valuable tool for ongoing water resource assessments.

8. This study utilized geostatistical maps and sequential Gaussian simulation to identify spatial variability and reduce mapping uncertainty. These techniques pinpointed suitable irrigation zones and areas requiring management interventions, supporting precision agriculture initiatives.

Future research could focus on evaluating the effectiveness of specific management practices in areas at risk of high salinity and sodicity, aiming to identify best practices for mitigating these challenges. Additionally, engaging with local farmers and stakeholders provides valuable insights into the practical challenges associated with groundwater use and management, fostering more participatory solutions.

**Author Contributions:** Conceptualization, T.A.B.A. and A.A.A.M.; methodology, T.A.B.A., A.A.A.M., A.A.C. and C.W.L.A.F.; software, T.A.B.A., A.A.A.M. and A.A.C.; validation, T.A.B.A., A.A.A.M. and A.A.C.; formal analysis T.A.B.A., A.A.A.M., J.L.M.P.d.L., A.L.R.d.P. and A.A.C.; investigation, T.A.B.A., A.A.A.M. and A.A.C.; resources, A.A.A.M.; data curation, T.A.B.A., J.L.M.P.d.L., C.W.L.A.F., A.L.R.d.P. and A.A.A.M.; writing—original draft preparation, T.A.B.A. and C.W.L.A.F.; writing—review and editing, T.A.B.A., A.A.A.M., J.L.M.P.d.L. and C.W.L.A.F.; visualization, T.A.B.A. and A.A.A.M.; supervision, A.A.A.M., J.L.M.P.d.L. and C.W.L.A.F.; project administration, A.A.A.M. and J.L.M.P.d.L.; funding acquisition, A.A.A.M. and J.L.M.P.d.L. All authors have read and agreed to the published version of the manuscript.

**Funding:** The National Council for Scientific and Technological Development—CNPq (151969/2020-5, and 311.588/2023-9); The Brazilian Funding Authority for Studies and Projects—FINEP; the Foundation of Science and Technology Support for Pernambuco State—FACEPE (“Tecnologias Hídricas para o Semiárido” Project—Grant APQ 0300-5.03/17, and BFP-0092-5.03/24). This research work was partly financed by National Funds through the FCT—Fundação para a Ciência e a Tecnologia (Portuguese Foundation for Science and Technology), credited to MARE <https://doi.org/10.54499/UIDB/04292/2020> (accessed on 6 september 2024) and <https://doi.org/10.54499/UIDP/04292/2020> (accessed on 6 september 2024) and to ARNET <https://doi.org/10.54499/LA/P/0069/2020> (accessed

on 6 september 2024) funded by the Portuguese Foundation for Science and Technology (FCT) through projects UIDB/04292/2020 and UIDP/04292/2020 granted to the Marine and Environmental Sciences Centre (MARE), University of Coimbra (Portugal), and the Associate Laboratory Aquatic Research Network (ARNET) supported by national funds.

**Data Availability Statement:** The data presented in this study are available upon request from the corresponding author.

**Acknowledgments:** We are grateful for the Postgraduate Program in Agricultural Engineering (PGEA) of the Federal Rural University of Pernambuco (UFRPE) for supporting the development of this research.

**Conflicts of Interest:** The authors declare no conflicts of interest.

## References

- Li, X.; Wu, H.; Qian, H.; Gao, Y. Groundwater Chemistry Regulated by Hydrochemical Processes and Geological Structures: A Case Study in Tongchuan, China. *Water* **2018**, *10*, 338. [[CrossRef](#)]
- Patel, M.P.; Gami, B.; Patel, A.; Patel, P.; Patel, B. Climatic and Anthropogenic Impact on Groundwater Quality of Agriculture Dominated Areas of Southern and Central Gujarat, India. *Groundw. Sustain. Dev.* **2020**, *10*, 100306. [[CrossRef](#)]
- Jamaa, H.; El Achheb, A.; Namr, K.I. Spatial Variation of Groundwater Quality and Assessment of Water Table Fluctuations in Plio-Quaternary Aquifer Formations in Doukkala Plain, Morocco. *Groundw. Sustain. Dev.* **2020**, *11*, 100398. [[CrossRef](#)]
- Almeida, T.A.B.; Montenegro, A.A.A.; Mackay, R.; Montenegro, S.M.G.L.; Coelho, V.H.R.; de Carvalho, A.A.; da Silva, T.G.F. Hydrogeological Trends in an Alluvial Valley in the Brazilian Semiarid: Impacts of Observed Climate Variables Change and Exploitation on Groundwater Availability and Salinity. *J. Hydrol. Reg. Stud.* **2024**, *53*, 101784. [[CrossRef](#)]
- Montenegro, A.A.A.; Montenegro, S.M.G.L. Variabilidade espacial de classes de textura, salinidade e condutividade hidráulica de solos em planície aluvial. *Rev. Bras. De Eng. Agrícola E Ambient.* **2006**, *10*, 30–37. [[CrossRef](#)]
- Masoud, A.A.; El-Horiny, M.M.; Atwia, M.G.; Gemal, K.S.; Koike, K. Assessment of Groundwater and Soil Quality Degradation Using Multivariate and Geostatistical Analyses, Dakhla Oasis, Egypt. *J. Afr. Earth Sci.* **2018**, *142*, 64–81. [[CrossRef](#)]
- Rivetti, M.O.; Budimir, L.; Mannix, N.; Miller, A.V.B.; Addizon, M.J.; Moyo, P.; Wanangwa, G.J.; Phiri, O.L.; Songola, C.E.; Nhlema, M.; et al. Responding to salinity in a rural African alluvial valley aquifer system: To boldly go beyond the world of hand-pumped groundwater supply? *Sci. Total Environ.* **2019**, *653*, 1005–1024. [[CrossRef](#)]
- Faraj, T.; Ragab, A.; El Alfy, M. Geochemical and hydrogeological factors influencing high levels of radium contamination in groundwater in arid regions. *Environ. Res.* **2020**, *184*, 109356. [[CrossRef](#)]
- Pazand, K.; Khosravi, D.; Ghaderi, M.R.; Rezvanianzadeh, M.R. Identification of the hydrogeochemical processes and assessment of groundwater in a semiarid region using major ion chemistry: A case study of Ardestan basin in Central Iran. *Groundw. Sustain. Dev.* **2018**, *6*, 245–254. [[CrossRef](#)]
- Andrade, T.S.; Montenegro, S.M.G.L.; Montenegro, A.A.A.; Rodrigues, D.F.B. Variabilidade espaço-temporal da condutividade elétrica da água subterrânea na região semiárida de Pernambuco. *Rev. Bras. De Eng. Agrícola E Ambient.* **2012**, *16*, 496–504. [[CrossRef](#)]
- Pattnaik, S.; Reddy, M.V. Bioconversion of municipal (organic) solid waste into nutrient rich vermicompost by earthworms (*Eudrilus eugeniae*, *Eisenia fetida* and *Perionyx excavatus*). *Dyn. Soil Dyn. Plant* **2009**, *3*, 122–128.
- Kumar, S.; Sanguetha, B. Assessment of groundwater quality in Madurai city by using geospatial techniques. *Groundw. Sustain. Dev.* **2020**, *10*, 100348. [[CrossRef](#)]
- Ielpo, P.; Leardi, R.; Pappagallo, G.; Uricchio, V.F. Tools based on multivariate statistical analysis for classification of soil and groundwater in Apulian agricultural sites. *Environ. Sci. Pollut. Res.* **2017**, *24*, 13967–13978. [[CrossRef](#)] [[PubMed](#)]
- Boufekane, A.; Saighi, O. Assessing groundwater quality for irrigation using geostatistical methods—Case of Wadi Nil Plain (North-East Algeria). *Groundw. Sustain. Dev.* **2019**, *8*, 179–186. [[CrossRef](#)]
- Delbari, M.; Motlagh, M.B.; Kiani, M.; Amiri, M. Investigating spatio-temporal variability of groundwater quality parameters using geostatistics and GIS. *Int. Res. J. Appl. Basic Sci.* **2013**, *4*, 3623–3632.
- Falowo, O.O. Irrigation and drinking water quality index determination for groundwater quality evaluation in Akoko Northwest and Northeast areas of Ondo State, Southwestern Nigeria. *Am. J. Water Sci. Eng.* **2017**, *3*, 66–73. [[CrossRef](#)]
- Wang, J.; Zhao, J.; Lei, X.; Wang, H. New approach for point pollution source identification in rivers based on the backward probability method. *Environ. Pollut.* **2018**, *241*, 759–774. [[CrossRef](#)]
- Moghaddam, M.B.; Mazaheri, M.; Samani, J.M.V. Inverse modeling of contaminant transport for pollution source identification in surface and groundwaters: A review. *Groundw. Sustain. Dev.* **2021**, *15*, 100651. [[CrossRef](#)]

19. Bodrud-Doza, M.; Islam, A.R.M.; Ahmed, F.; Das, S.; Saha, N.; Rahman, M.S. Characterization of groundwater quality using water evaluation indices, multivariate statistics, and geostatistics in central Bangladesh. *Natl. Water Res. Cent.* **2016**, *30*, 19–40. [[CrossRef](#)]
20. Delbari, M.; Amiri, M.; Motlagh, M.B. Assessing groundwater quality for irrigation using the indicator kriging method. *Appl. Water Sci.* **2016**, *6*, 371–381. [[CrossRef](#)]
21. Zhao, Y.; Xu, X.; Huang, B.; Sun, W.; Shao, X.; Shi, X.; Ruan, X. Using robust Kriging and sequential gaussian simulation to delineate the copper- and lead-contaminated areas of a rapidly industrialized city in Yangtze River delta, China. *Environ. Geol.* **2007**, *52*, 1423–1433. [[CrossRef](#)]
22. Delbari, M.; Afsariab, P.; Loiskandl, W. Using sequential gaussian simulation to assess the field-scale spatial uncertainty of soil water content. *Catena* **2009**, *79*, 163–169. [[CrossRef](#)]
23. Goovaerts, P. *Geostatistics for Natural Resources Evaluation*; Oxford University Press: New York, NY, USA, 1997.
24. Sousa, L.B.; de Assunção Montenegro, A.A.; da Silva, M.V.; Almeida, T.A.B.; de Carvalho, A.A.; da Silva, T.G.F.; de Lima, J.L.M.P. Spatiotemporal analysis of rainfall and droughts in a semiarid basin of Brazil: Land use and land cover dynamics. *Remote Sens.* **2023**, *15*, 2550. [[CrossRef](#)]
25. Almeida, T.A.B.; Montenegro, A.A.A.; da Silva, R.A.B.; de Lima, J.L.M.P.; Carvalho, A.A.; da Silva, J.R.L. Evaluating Daily Water Stress Index (DWSI) Using Thermal Imaging of Neem Tree Canopies under Bare Soil and Mulching Conditions. *Remote Sens.* **2024**, *16*, 2782. [[CrossRef](#)]
26. Qu, M.K.; Li, W.D.; Zhang, C.R. Assessing the risk costs in delineating soil nickel contamination using sequential Gaussian simulation and transfer functions. *Ecol. Inform.* **2013**, *13*, 99–105. [[CrossRef](#)]
27. Guadagnini, L.; Menafoglio, A.; Sanchez-Vila, X.; Guadagnini, A. Probabilistic assessment of spatial heterogeneity of natural background concentrations in large-scale groundwater bodies through Functional Geostatistics. *Sci. Total Environ.* **2020**, *720*, 140139. [[CrossRef](#)]
28. Li, J.; Wang, D.; Li, D.; Wu, P.; Huang, X. Hydrogeological structure modelling based on an integrated approach using multi-source data. *J. Hydrol.* **2021**, *600*, 126435. [[CrossRef](#)]
29. Fontes Júnior, R.V.d.P.; Montenegro, A.A.d.A. Dependência temporal de potenciometria e salinidade de aquífero aluvial com a precipitação e evapotranspiração. *Rev. Bras. De Recur. Hídric.* **2017**, *22*, 1–9. [[CrossRef](#)]
30. Montenegro, S.M.G.L.; Montenegro, A.A.A.; Mackay, R.; Oliveira, A.S.C. Dinâmica hidro-salina em aquífero aluvial utilizado para agricultura irrigada familiar em região semiárida. *Rev. Bras. Recur. Hídricas* **2003**, *8*, 85–92.
31. Corrêa, M.M.; Ribeiro, M.R. *Levantamento detalhado de solos da Fazenda Nossa Senhora do Rosário (Pesqueira-PE)*; UFRPE/UFPE/CNPq/BNB: Recife, Brazil, 2001; 35p, Relatório Técnico.
32. Allen, R.G.; Pereira, L.S.; Raes, D.; Smith, M. Crop Evapotranspiration—Guidelines for Computing Crop Water Requirements. In *FAO Irrigation and Drainage Paper 56*, 1st ed.; FAO: Rome, Italy, 1998; pp. 1–297.
33. Sawyer, G.N.; McCarthy, D.L. *Chemistry of Sanitary Engineers*, 2nd ed.; McGraw Hill: New York, NY, USA, 1967; 518p.
34. Todd, D.K. *Ground Water Hydrology*, 2nd ed.; John Wiley and Sons Inc.: New York, NY, USA, 1980; pp. 10–138.
35. Ayers, R.S.; Westcot, D.W. *A Qualidade da Água na Agricultura*; UFPB: Campina Grande, Brazil, 1999; 153p, Estudos FAO: Irrigação e Drenagem, 29.
36. Richards, L.A. *Diagnosis and Improvement of Saline and Alkali Soils*; US Department of Agriculture: Washington, DC, USA, 1954; USDA Agricultural Handbook 60; 160p.
37. Adimalla, N. Groundwater Quality for Drinking and Irrigation Purposes and Potential Health Risks Assessment: A Case Study from Semiarid Region of South India. *Expo. Health* **2019**, *11*, 109–123. [[CrossRef](#)]
38. Warrick, A.W.; Nielsen, D.R. Spatial Variability of Soil Physical Properties in the Field. In *Applications of Soil Physics*; Hillel, D., Ed.; Academic Press: New York, NY, USA, 1980; pp. 319–334.
39. Hoaglin, D.C.; Mosteller, F.; Tukey, J.W. *Análise Exploratória de Dados: Técnicas Robustas*; Salamandra: Lisboa, Portugal, 1992; 446p.
40. Journel, A.G. *Fundamentals of Geostatistics in Five Lessons*; American Geophysical Union: Washington, DC, USA, 1989; 40p.
41. Webster, R.; Oliver, M.A. *Geostatistics for Environmental Scientists*, 2nd ed.; Wiley: Chichester, UK, 2007.
42. Cambardella, C.A.; Moorman, T.B.; Novak, J.M.; Parkin, T.B.; Karlen, D.L.; Turco, R.F.; Kornopka, A.E. Field-Scale Variability of Soil Properties in Central Iowa Soils. *Soil Sci. Soc. Am. J.* **1994**, *58*, 1501–1511. [[CrossRef](#)]
43. Golden Software. *Surfer for Windows Version 9.0*; Golden Software: Golden, CO, USA, 2010; 66p.
44. Fontes Júnior, R.V.P.; Montenegro, A.A.A.; Montenegro, S.M.G.L.; Santos, T.E.M. Estabilidade Temporal da Potenciometria e da Salinidade em Vale Aluvial no Semiárido de Pernambuco. *Rev. Bras. De Eng. Agrícola E Ambient.* **2012**, *16*, 1188–1197. [[CrossRef](#)]
45. Kim, M.J.; Nriagu, J.; Haack, S. Arsenic Species and Chemistry in Groundwater of Southeast Michigan. *Environ. Pollut.* **2002**, *20*, 379–390. [[CrossRef](#)] [[PubMed](#)]
46. Adebayo, T.B.; Abegunrin, T.P.; Awe, G.O.; Are, K.S.; Guo, H.; Onofua, O.E.; Adegbola, G.A.; Ojediran, J.O. Geospatial Mapping and Suitability Classification of Groundwater Quality for Agriculture and Domestic Uses in a Precambrian Basement Complex. *Groundw. Sustain. Dev.* **2021**, *12*, 100497. [[CrossRef](#)]

47. Lima, A.d.O.; Lima-Filho, F.P.; Dias, N.d.S.; Chipana-Rivera, R.; Neto, M.F.; Souza, A.d.M.; Rego, P.R.D.A.; Fernandes, C.d.S. Variation of the water table and salinity in alluvial aquifers of underground dams in the semi-arid region of Rio Grande do Norte, Brazil. *Biosci. J.* **2019**, *35*, 477–484. [[CrossRef](#)]
48. Nouayti, N.; Khattach, D.; Hilali, M. Evaluation de la qualité physico-chimique des eaux souterraines des nappes du JuSARsique du haut bassin de Ziz (Haut Atlas central, Maroc) Assessment of physico-chemical quality of groundwater of the JuSARsic aquifers in high basin of Ziz (Central High Atlas, Morocco). *J. Mater. Environ. Sci.* **2015**, *6*, 1068–1071.
49. Tomaz, A.; Palma, P.; Fialho, S.; Lima, A.; Alvarenga, P.; Potes, M.; Salgado, R. Spatial and Temporal Dynamics of Irrigation Water Quality under Drought Conditions in a Large Reservoir in Southern Portugal. *Environ. Monit. Assess.* **2020**, *192*, 93. [[CrossRef](#)]
50. Batarseh, M.; Imreizeeq, E.; Tilev, S.; Al Alaween, M.; Suleiman, W.; Al Remeithi, A.M.; Al Tamimi, M.K.; Al Alawneh, M. Assessment of Groundwater Quality for Irrigation in the Arid Regions Using Irrigation Water Quality Index (IWQI) and GIS-Zoning Maps: Case Study from Abu Dhabi Emirate, UAE. *Groundw. Sustain. Dev.* **2021**, *14*, 100611. [[CrossRef](#)]
51. Taloor, A.K.; Pir, R.A.; Adimalla, N.; Ali, S.; Manhas, D.S.; Roy, S.; Singh, A.K. Spring Water Quality and Discharge Assessment in the Basantar Watershed of Jammu Himalaya Using Geographic Information System (GIS) and Water Quality Index (WQI). *Groundw. Sustain. Dev.* **2020**, *10*, 100364. [[CrossRef](#)]
52. Bai, T.; Tahmasebi, P. Sequential Gaussian Simulation for Geosystems Modeling: A Machine Learning Approach. *Geosci. Front.* **2021**, *13*, 101258. [[CrossRef](#)]
53. Karami, S.; Jalali, M.; Karami, A.; Katibeh, H.; Fatehi Marj, A. Evaluating and Modeling the Groundwater in Hamedan Plain Aquifer, Iran, Using the Linear Geostatistical Estimation, Sequential Gaussian Simulation, and Turning Band Simulation Approaches. *Model. Earth Syst. Environ.* **2022**, *8*, 3555–3576. [[CrossRef](#)]

**Disclaimer/Publisher’s Note:** The statements, opinions and data contained in all publications are solely those of the individual author(s) and contributor(s) and not of MDPI and/or the editor(s). MDPI and/or the editor(s) disclaim responsibility for any injury to people or property resulting from any ideas, methods, instructions or products referred to in the content.